Inflammatory Manifestations of Experimental Lymphatic Insufficiency

Raymond Tabibiazar[1], Lauren Cheung[1], Jennifer Han[1], Jeffrey Swanson[1], Andreas Beilhack[1], Andrew An[1], Soheil S. Dadras[2], Ned Rockson[1], Smita Joshi[1], Roger Wagner[1], Stanley G. Rockson[1*]

1 Stanford Center for Lymphatic and Venous Disorders, Division of Cardiovascular Medicine, Stanford University School of Medicine, Stanford, California, United States of America, **2** Department of Pathology, Stanford University School of Medicine, Stanford, California, United States of America

Funding: The authors gratefully acknowledge grant support from the Susan G. Komen Breast Cancer Foundation and the Western States Affiliate of the American Heart Association. The funders had no role in study design, data collection and analysis, decision to publish, or preparation of the manuscript.

Competing Interests: The authors have declared that no competing interests exist.

Academic Editor: Patrick Vallance, University College London, United Kingdom

Citation: Tabibiazar R, Cheung L, Han J, Swanson J, Beilhack A, et al. (2006) Inflammatory manifestations of experimental lymphatic insufficiency. PLoS Med 3(7): e254. DOI: 10.1371/journal.pmed.0030254

Received: June 8, 2005
Accepted: April 5, 2006
Published: July 18, 2006

DOI: 10.1371/journal.pmed.0030254

Abbreviations: dpm, disintegrations per minute; EST, expressed sequence tag; FDR, false detection rate; GO, Gene Ontology; *luc*, *luciferase*; qRT-PCR, quantitative real-time RT-PCR; SAM, significance analysis of microarrays

* To whom correspondence should be addressed. E-mail: srockson@cvmed.stanford.edu

ABSTRACT

Background

Sustained lymph stagnation engenders a pathological response that is complex and not well characterized. Tissue inflammation in lymphedema may reflect either an active or passive consequence of impaired immune traffic.

Methods and Findings

We studied an experimental model of acute post-surgical lymphedema in the tails of female hairless, immunocompetent SKH-1 mice. We performed in vivo imaging of impaired immune traffic in experimental, murine acquired lymphatic insufficiency. We demonstrated impaired mobilization of immunocompetent cells from the lymphedematous region. These findings correlated with histopathological alterations and large-scale transcriptional profiling results. We found intense inflammatory changes in the dermis and the subdermis. The molecular pattern in the RNA extracted from the whole tissue was dominated by the upregulation of genes related to acute inflammation, immune response, complement activation, wound healing, fibrosis, and oxidative stress response.

Conclusions

We have characterized a mouse model of acute, acquired lymphedema using in vivo functional imaging and histopathological correlation. The model closely simulates the volume response, histopathology, and lymphoscintigraphic characteristics of human acquired lymphedema, and the response is accompanied by an increase in the number and size of microlymphatic structures in the lymphedematous cutaneous tissues. Molecular characterization through clustering of genes with known functions provides insights into processes and signaling pathways that compose the acute tissue response to lymph stagnation. Further study of genes identified through this effort will continue to elucidate the molecular mechanisms and lead to potential therapeutic strategies for lymphatic vascular insufficiency.

The Editors' Summary of this article follows the references.

Introduction

Acquired lymphedema is a common, important, and often devastating consequence of successful surgical and adjuvant therapy of breast cancer and other malignancies [1,2]. The biology of regional lymphatic vascular insufficiency (lymphedema) is complex and, as yet, poorly understood. Consequently, there is a paucity of effective treatment strategies in patients with lymphedema [2]. There is an obvious need for better molecular characterization of this disease process to elucidate the pathobiology of lymphatic vascular insufficiency.

The tissue response to lymph stagnation is rather complex. The profound structural and functional abnormalities in the lymphedematous tissues reflect a multicellular response to impaired extracellular fluid mobilization [3]. It has been suggested that lymphedema provokes an inflammatory tissue response in the skin [4]. While it is conceivable that the inflammatory nature of the tissue response to lymph stagnation reflects either the active or passive consequences of impaired immune traffic [5], direct experimental confirmation is lacking.

Transcriptional profiling has been utilized in the molecular characterization of isolated lymphatic endothelia [6,7], but the molecular end-organ response to lymph stagnation remains unaddressed and poorly understood. While lymphatic and blood vessel responses to injury might be predictable, an elucidation of whole tissue response to disease is likely to provide more relevant insights into the important interactions between the tissue matrix and the resident, heterogeneous cellular populations that likely compose the target-organ response to persistent lymph stagnation.

To investigate tissue responses to lymphatic vascular insufficiency, we have undertaken dynamic, in vivo imaging of the impaired immune traffic in a murine model of acquired lymphatic insufficiency that is intended to simulate, in part, the lymphatic dysfunction of post-surgical lymphedema [8]. These observations were correlated with an assessment of the cutaneous histopathology in the lymphedema tissue. Furthermore, to investigate the molecular mechanisms of tissue response to lymphatic vascular insufficiency, we have undertaken a large-scale transcriptional profiling of the lymphedema tissue utilizing a comprehensive mouse cDNA microarray containing 42,300 features, representing over 25,000 unique genes and expressed sequence tags (ESTs) [9]. The patterns of gene expression in lymphedema were contrasted with those observed in normal and surgical sham controls.

Methods

This study was approved by the Administrative Panels on Laboratory Animal Care of Stanford University.

Creation of Experimental Lymphedema

Post-surgical lymphedema was experimentally created in the tails of female hairless, immunocompetent SKH-1 mice (Charles River Laboratories, Boston, Massachusetts, United States). Prior to surgery, the mice were anesthetized with intraperitoneal injection of 0.07 cc of a solution containing ketamine, xylazine, and saline. For each intervention, the skin of the tail was circumferentially incised proximally, at a point 16 mm distal to its base. The major lymphatic trunks were identified through subcutaneous injection of methylene blue distal to the surgical incision, followed by controlled, limited cautery ablation of these structures. In surgical controls (sham animals), skin incision alone was performed, with methylene blue injection but without lymphatic cautery. The normal control animals did not undergo any surgical manipulation. All animal subjects were sacrificed on day 14 of observation. After sacrifice, 0.5-gm sections of the tail were harvested for paraffin embedding and RNA extraction.

Tail Volume Quantitation

Tail volume was quantitated in each animal subject immediately prior to sacrifice. Volumetric assessment was performed with a manually adjusted caliper, with serial measurement of the tail circumference at 5-mm intervals along its axis. The tail volume was quantitated with the truncated cone formula [10].

Histology

Immediately following sacrifice, 0.5-gm sections of the tail were harvested for histological analysis and RNA extraction. Sections extended from a point 4 mm proximal to the surgical incision to 8 mm beyond it. For examination of the responses remote from the point of injury, sections were harvested 4 cm distal to the surgical site. The specimens were fixed overnight in 4% paraformaldehyde. After paraffin embedding, 5-μm sections were stained with hematoxylin and eosin (Richard-Allan Scientific, Kalamazoo, Michigan, United States). For visualization of histiocytes/mast cells, the sections were stained with a 1% toluidine blue solution (LabChem, Pittsburgh, Pennsylvania, United States) diluted in 1% NaCl. After deparaffinization in xylene, sections were rehydrated though a series of graded alcohol steps starting with 100% EtOH and ending in 50% EtOH. Slides remained in toluidine blue for 2 min and were then dehydrated through graded alcohol washes and covered with Cytoseal (Richard-Allan Scientific).

LYVE-1 Immunohistochemical Staining

Paraffin sections 5 μm thick were deparaffinized in xylene, rehydrated in a graded series of ethanol, pretreated with target retrieval solution (Dako, Carpinteria, California, United States) in a pressure cooker, and incubated in a peroxidase block for 10 min. Sections were then incubated with rabbit polyclonal anti-LYVE-1 antibody (1:200, Upstate Cell Signaling Solutions, Lake Placid, New York, United States) for 1 h at room temperature, followed by horseradish-peroxidase-conjugated secondary antibody for 30 min at room temperature and detection with DAB for 4 min (Envision System Kit, Dako). Tissue sections were counterstained with Gill 1 hematoxylin (Richard-Allan Scientific) for 15 s, then dehydrated in graded ethanol and coverslipped with CoverSafe (American Master*Tech Scientific, Lodi, California, United States).

Functional Imaging of Immune Traffic in the Lymphedema Model

Experimental lymphedema was created surgically in the tails of FVB/N female wild-type mice (Jackson Laboratory, Bar Harbor, Maine, United States; $n = 3$), using the technique described above. Surgical sham controls ($n = 5$) were also

created and compared with normal mice ($n = 5$). For in vivo bioluminescence imaging, spleens from transgenic luciferase (*luc*$^+$) heterozygous animals were put into single-cell suspension, expressing firefly *luc* under the control of a chicken beta-actin promoter as previously described [11,12]. The single-cell suspensions from mouse spleens consisted of different hematopoietic lineages: ~40% were CD19+ B cells, ~20% were CD4+ T cells, ~10%–15% were CD8+ T cells, 3% were NK1.1+ NK cells, and the rest were GR.1+ granulocytes, Mac-1+ macrophages, CD11c+ dendritic cells, and rarer cell populations. A total of 4×10^6 splenocytes (>97% CD45+) in PBS were injected in a volume of 20 ml into the tail interstitium, 1 cm caudal to the site of surgery, in both lymphedema mice and surgical shams. Normal mice were injected at the corresponding level of the tail. Injections were performed on post-surgical day 7. Thereafter, *luc*$^+$ cells were repetitively imaged in vivo, at predetermined intervals following the cell injections. In brief, mice were anesthetized by intraperitoneal co-injection of a mixture of ketamine (1 mg/mouse), xylazine (μg/mouse) in PBS, and the substrate luciferin (150 mg/kg).

Ten minutes thereafter, dorsal images were obtained with an IVIS100 CCD imaging system (Xenogen, Alameda, California, United States). The efficiency of cellular lymphatic drainage was determined by direct imaging of light emission at each of the measured time points, with quantitation of the change in light emission relative to that observed 20 h after cell injection, which was defined as 100%.

Microsphere Quantitation of Arterial Perfusion of the Mouse Tail

The arterial perfusion of the tails of experimental and control mice was quantitated through intracardiac microsphere injection. After induction of general anesthesia, stable-labeled 15-μm microspheres (STERIspheres Gold, BioPAL, Worcester, Massachusetts, United States) were injected into the left ventricle. Each animal subject received 0.5×10^6 microspheres (0.2 ml) injected directly into the left ventricle. The animals were sacrificed after 12 min. The tails were harvested and dried overnight at 70 °C. The assay to quantitate disintegrations per minute (dpm) was performed by BioPhysics Assay Laboratory (Worcester, Massachusetts, United States) as previously described [13].

Lymphoscintigraphy in Experimental Lymphedema

Whole body lymphoscintigraphy was performed after the intradermal injection of 100 μCi/0.02 ml of filtered ^{99m}Tc-sulfur colloid (100 nm size) into the tip of the tail. Dynamic and static images (255×255) were acquired using a parallel hole collimator in a microSPECT gamma camera (Lumigem, Gamma Medica, Northridge, California, United States). The dynamic images (1,000 frames; 0.5 s/frame) were started 60 s prior to the injection of the tracer. The injection lasted for 20 s. The static images (10 min) were acquired immediately after the dynamic acquisition.

Microarray Experimental Design, RNA Preparation, and Hybridization

Tissues were derived from nine mice for each of the three biological states under study (cutaneous specimens from normal, lymphedematous, and surgical sham animals), for a total of 27 mice. All microarray hybridizations were performed with three biological replicates, using pooled samples independently derived from three mice each, for a total of nine hybridizations. After tissue was harvested for histological examination, the remaining, distal portion of the tail was retrieved for RNA isolation. After completely separating the tail skin from the cartilage by blunt dissection, the tissue was separated into segments of 0.5 mm for further processing. Total RNA was isolated using a modified two-step purification protocol as described previously [14]. RNA integrity was assessed using the Agilent 2100 Bioanalyzer System with RNA 6000 Pico LabChip Kit (Agilent, Palo Alto, California, United States). First-strand cDNA was synthesized from 15 μg of total RNA derived from each pool and from whole embryonic-day-17.5 embryo for reference RNA, in the presence of Cy3 and Cy5 dUTP, respectively, and hybridized to the Mouse Transcriptome Microarray [14–16]. A continuously updated and annotated list of the cDNAs included on this array is available at the Stanford Microarray Database [17] (Table S1).

Data Acquisition, Analysis, and Statistical Analysis

Image acquisition of the mouse cDNA microarrays was performed on an Agilent G2565AA Microarray Scanner System. Feature extraction was performed with GenePix 4.0 software (Bucher Biotec, Basel, Switzerland). Numerical raw data were migrated from GenePix, without processing, into an Oracle relational database (CoBi) that was designed specifically for microarray data analysis (GeneData, Basel, Switzerland). The data were then analyzed using Expressionist software (GeneData). After background subtraction and dye normalization, features with low signal intensity in the reference channel were filtered if signal was less than 2.5× background value, retaining a total of 8,353 features for further analysis. *K*-nearest-neighbor algorithm was applied to impute for missing values (<7% of remaining data) [18]. For two-group comparisons, we used the significance analysis of microarrays (SAM) algorithm [19,20]. Heat maps were generated using HeatMap Builder [21,22]. For enrichment analysis we used the EASE analysis software, which uses Gene Ontology (GO) annotation and Fisher's exact test to derive biological themes within particular gene sets [23].

Quantitative Real-Time RT-PCR

Quantitative real-time RT-PCR (qRT-PCR) was performed as described [14]. Primers and probes for ten representative differentially expressed genes were obtained from Applied Biosystems Assays-on-Demand (Applied Biosystems, Foster City, California, United States. cDNA was synthesized from 5 μg of total RNA using Taqman Reverse Transcription Reagents (Applied Biosystems), a set which includes MultiScribe reverse transcriptase, RNase inhibitor, dNTP mixture, oligo $d(T)_{16}$, random hexamers, 10× RT buffer, and $MgCl_2$ solution. Amplification was performed in triplicate at 50 °C for 2 min and 95 °C for 10 min, followed by 40 cycles of 95 °C for 15 s and 60 °C for 1 min. Reactions without template and/or enzyme were used as negative controls. 18S ribosomal RNA was used as an internal control. A standard curve derived from embryonic-day-17.5 mouse RNA was plotted for each target gene by linear regression using SPSS version 11.0 software (Applied Biosystems). RNA quantity was expressed relative to the corresponding 18S control. Fold differences were calculated by dividing the experimental results by the

Table 1. Primer/Probe Sequences for the Taqman-Based qRT-PCR

Gene Name	Forward Primers	Reverse Primers	Taqman Probes
calgranulin A	GACTTCAAGAAAATGGTCACTACTGAGT	TGTCCAATTCTCTGAACAAGTTTTCGA	FAM-TCAGTTTGTGCAGAATAT-NFQ
calgranulin B	AGACAAATGGTGGAAGCACAGTT	CCAGGTCCTCCATGATGTCATTTAT	FAM-TTCTCTTTCTTCATAAAGGTTGCC-NFQ
clusterin	AGGGCGAAGACAAGTACTACCTT	CACCACCACCTCAGTGACA	FAM-CCACCGTGACCACCC-NFQ
MMP3	TCCCGTTTCCATCTCTCTCAAGA	GGGTACCACGAGGACATCAG	FAM-TCCCTCTATGGAACTCC-NFQ
MMP14	CCCAAGGCAGCAACTTCAG	CCTGGAGGTAGGTAGCCATACTG	FAMCCCGAAGCCTGGCTGC-NFQ

DOI: 10.1371/journal.pmed.0030254.t001

pooled normal results and were plotted on a log10 scale. The primers and probes utilized in this study are listed in Tables 1 and 2.

Results

Murine Model of Acute Experimental Lymphedema: Tail Volume Quantification

Forty-five 3-wk-old SKH-1 hairless mice were studied in this investigation. Of these, 18 underwent post-surgical lymphatic ablation, nine served as surgical sham controls, and the remaining 18 served as normal controls. Tail volume for each group of animals is depicted in Figure 1. At post-surgical day 7, the lymphedema tail volumes were 200% ± 50% of baseline ($p < 0.008$ when compared to surgical sham controls). In the animals subjected to lymphatic ablation, the edematous enlargement of the tails persisted until the day of sacrifice (day 14). Of note is the fact that cutaneous healing of the wound, both in the lymphedematous and surgical sham subjects, was complete by day 14. There was no statistically significant change in tail volume in either surgical sham or normal controls.

Histological Assessment of the Cutaneous Response to Lymphatic Interruption

Hematoxylin and eosin specimens derived from the lymphedematous tails were characterized by the presence of marked acute inflammatory changes (Figure 2B), when compared to the tissue derived from the normal tails (Figure 2A). There was a notable increase in cellularity, with an increase in the number of observed fibroblasts and histiocytes, as well as a large infiltration of neutrophils Granulation tissue was observed closer to the center of the section, with bystander destruction of muscle tissue. In addition, there was hyperkeratosis and spongiosis and edema of the epidermis, with irregularity of the epidermal/dermal junction, elongation of the dermal papillae, and a 2- to 3-fold expansion of tissue between the bone and the epidermis. Lymphedema specimens were characterized by the presence of numerous dilated lymphatics in the dermis and subdermis, as seen in Figure 2B. In contrast, normal tail sections were devoid of these dilated structures. The normal tissues were characterized by the presence of a thin dermis and epidermis, with a normal epidermal/dermal junction (Figure 2A). The surgical sham controls were indistinguishable from normals, with no increased cellularity in dermis or epidermis, and no enlarged nuclei or hyperkeratosis.

In order to assess whether the lymphedematous changes created a uniform pathological response distal to the point of lymphatic ablation, the tissues were also sampled distally (4 cm distal to the point of surgical incision) in normal (Figure 2C) and lymphedematous (Figure 2D) tails. The observed changes were comparable to those observed adjacent to the surgical site: lymphedematous tissues were characterized by hypercellularity, inflammatory infiltration, and microlymphatic dilatation that were not present in the normal tissues.

Table 2. Names of Taqman-Based qRT-PCR Probes

Symbol	Name	Applied Biosystems ID
Cdh11	*cadherin 11*	Mm00515462_m1
HADH2	*hydroxyacyl-coenzyme A dehydrogenase type II*	Mm00840109_m1
Myd88	*myeloid differentiation primary response gene 88*	Mm00440338_m1

DOI: 10.1371/journal.pmed.0030254.t002

Quantitative Assessment of Arterial Perfusion in the Murine Tail Lymphedema Model

While we took great care to avoid concurrent injury to adjacent vascular structures during surgical lymphatic ablation, we have undertaken an evaluation to exclude inadvertent arterial injury during surgery. The mouse tails remained grossly stable throughout the post-surgical observation phase, with no evidence of frank necrosis distal to the surgical site. In order to further substantiate the absence of an arterial ischemic contribution to the histological pathology observed in lymphedema, quantitative assessment of arterial perfusion was performed through intracardiac injection of stable 15-μm microspheres into the left ventricles of normal ($n = 3$) and lymphedema ($n = 3$) mice. Perfusion of the tail, measured in disintegrations per minute (dpm), did not differ statistically between the two categories (normal, 151,186 ± 69,213 dpm; sham, 95,581 ± 48,003 dpm), confirming preservation of arterial supply in the lymphedema animals.

LYVE-1 Immunohistochemical Staining

The nature of the lymphatic vascular response distal to the anatomic surgical ablation was assessed with quantitative assessment of lymphatic vessel number and size by immunohistochemical staining for LYVE-1(Figure 3) [24,25]. As observed in the hematoxylin and eosin sections, lymphedema was characterized by the presence of numerous dilated microlymphatic structures in the dermis and subdermis. Mean lymphatic vessel number was determined by averaging the number of total lymphatic vessels in all the fields of each slide

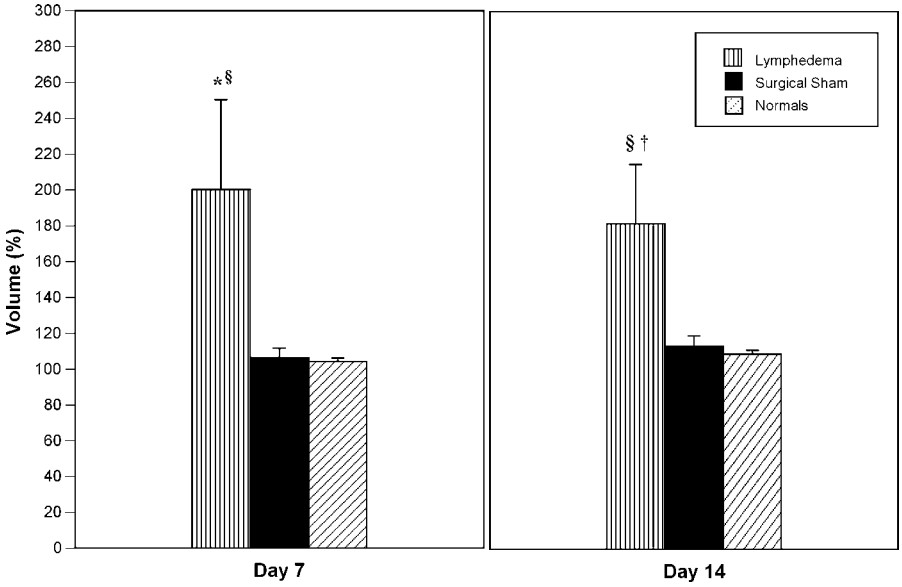

Figure 1. Tail Volume Changes at Post-Surgical Day 7 and at Day 14
DOI: 10.1371/journal.pmed.0030254.g001

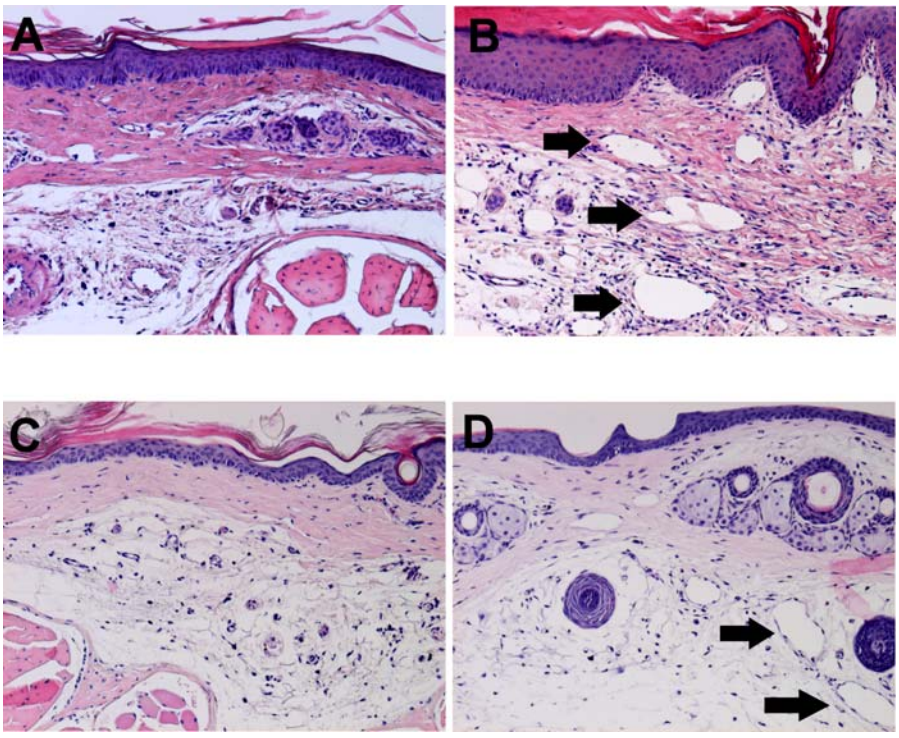

Figure 2. Histopathology of Experimental Lymphedema in the Murine Tail

Lymphedema was characterized by the presence of marked acute inflammatory changes, both adjacent to the surgical site and within distal regions of the tail, remote from the site of surgical ablation.

(A) Normal tail skin harvested 16 mm from the base of the tail is characterized by the presence of a thin dermis and epidermis, with a normal epidermal/dermal junction. Surgical sham controls were indistinguishable from normals, with no increased cellularity in dermis or epidermis, and no enlarged nuclei or hyperkeratosis.

(B) Lymphedematous skin harvested immediately distal to the site of prior surgical lymphatic ablation is characterized by the presence of marked acute inflammatory changes, absent in the tissue derived from the normal tails. There is a notable increase in cellularity, with an increase in the number of observed fibroblasts and histiocytes, as well as a large infiltration of neutrophils. There is hyperkeratosis and spongiosis and edema of the epidermis, with irregularity of the epidermal/dermal junction, elongation of the dermal papillae, and a 2- to 3-fold expansion of tissue between the bone and the epidermis. There are numerous dilated lymphatic microvessels in the dermis and subdermis (black arrows). In contrast, normal tail sections were devoid of these dilated structures.

(C) Normal skin derived from the distal tail. No inflammation, hypercellularity, or lymphatic dilatation is observed.

(D) Distal skin in lymphedema. Spongiosis and lymphatic microvascular dilatation (black arrows) are once again detectable.

DOI: 10.1371/journal.pmed.0030254.g002

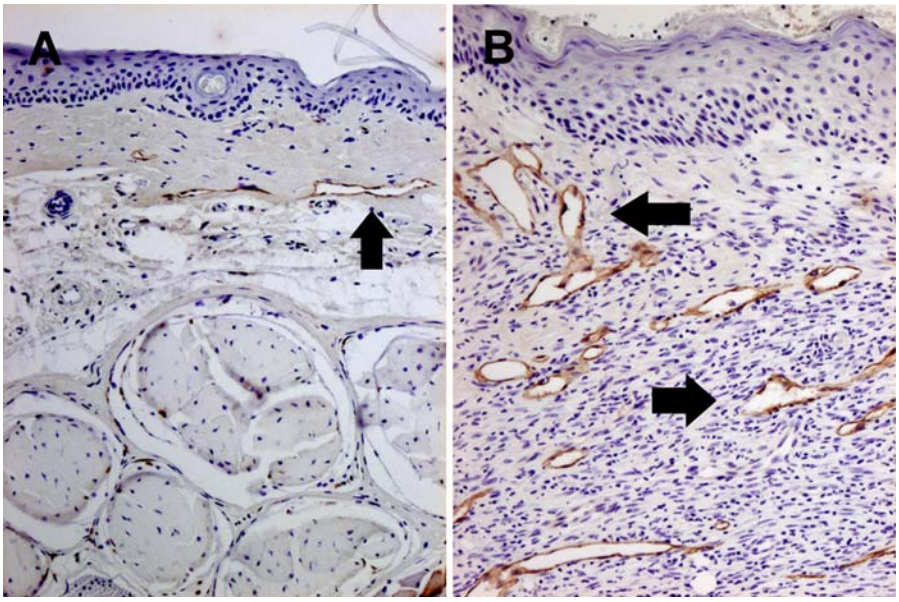

Figure 3. LYVE-1 Immunohistochemical Staining

Immunohistochemical staining for LYVE-1 is depicted in surgical sham controls (A) and in lymphedema (B) (black arrows). The lymphedema response is characterized by the presence of numerous dilated microlymphatic structures in the dermis and subdermis. Lymphedema produces a statistically significant increase in average cross-sectional vessel area.

DOI: 10.1371/journal.pmed.0030254.g003

at 10× magnification. Single brown-stained endothelial cells with a lumen were counted as individual lymphatic vessels. Quantitation was performed for normals ($n = 3$), surgical shams ($n = 3$), and lymphedema tails ($n = 3$). Lymphedema was characterized by an increase in LYVE-1-positive vessel number per field that was not observed in shams: lymphedema, 7.0 ± 4.8; sham, 0.6 ± 0.5; and normal, 1.2 ± 0.8.

Vessel area was quantitated according to the formula $\pi \cdot r_1 \cdot r_2$. The average lymphatic luminal area per field was 503 ± 158 μm^2 in normals, 436 ± 345 μm^2 in shams, and 51,344 ± 18,688 μm^2 in lymphedema. Normals and shams did not differ statistically, but the lymphedema group displayed a statistically significant increase in average vessel area when compared either to normals or to sham surgical animals ($p = 0.009$ for each comparison). Thus, in summary, the experimental lymphedema is accompanied by an increase in vessel number and, even more notably, by an increase in lymphatic vascular cross-sectional area.

Lymphoscintigraphy of Experimental Lymphedema

Whole body lymphoscintigraphy was performed in normal ($n = 4$) and lymphedema ($n = 4$) mice. All non-operated mice showed lymphatic drainage from the tip of the tail through two lumbar lymph nodes, asymmetric para-aortic nodes, and mediastinal nodes with final visualization of the liver. The lymphatic flow speed in basal conditions was estimated to be 0.9 ± 0.66 mm/s. In the lymphedema animals, significant dermal backflow was present, but no flow was observed beyond the base of the tail. These lymphoscintigraphic findings closely simulate the qualitative changes observed in the analogous imaging of acquired human lymphedema.

Functional In Vivo Imaging of Immune Traffic

The lymphatic vasculature participates in the immune response through the continuous transportation of white blood cells and antigen-presenting cells. The constellation of histological observations in this model, otherwise unexplained by impaired interstitial fluid mobilization, suggests that derangements in lymphatic immune traffic might contribute—actively, passively, or both ways—to the biology of lymph stagnation. Accordingly, we chose to corroborate histopathology with observed, quantifiable changes in immune traffic.

Bioluminescence imaging was performed on days 3, 5, and 7.5 following the introduction of luc^+ cells into the distal tail (corresponding to post-operative days 10, 12, and 17.5, respectively). In general, when compared to normals, the clearance of bioluminescent immunocytes was delayed in lymphedema, but remained unimpaired in the surgical sham controls. Figure 4 depicts a series of imaging experiments for a representative pair of lymphedema and normal control mice. Relative photon density, expressed as the percent of the observed value on day 1, was significantly greater in lymphedema than in the normals, both at day 3 and at day 7 post-injection (Figure 4).

Large-Scale Analysis of Cutaneous Gene Expression in Response to Lymphatic Vascular Insufficiency (Lymph Stasis)

cDNA microarrays containing a large portion of the mouse transcriptome were used to study the repertoire of genes expressed in the murine skin structures. Triplicate microarray experiments were performed using pooled RNA from the tail skin of female SKH-1 hairless mice representing three biological states: normal, lymphedematous, and surgical sham. Our analyses demonstrated significantly different patterns of gene expression in normal skin and the skin derived from lymphedematous mice. SAM, at a false detection rate (FDR) of 5%, identified 429 upregulated genes in the lymphedema state versus 183 downregulated genes

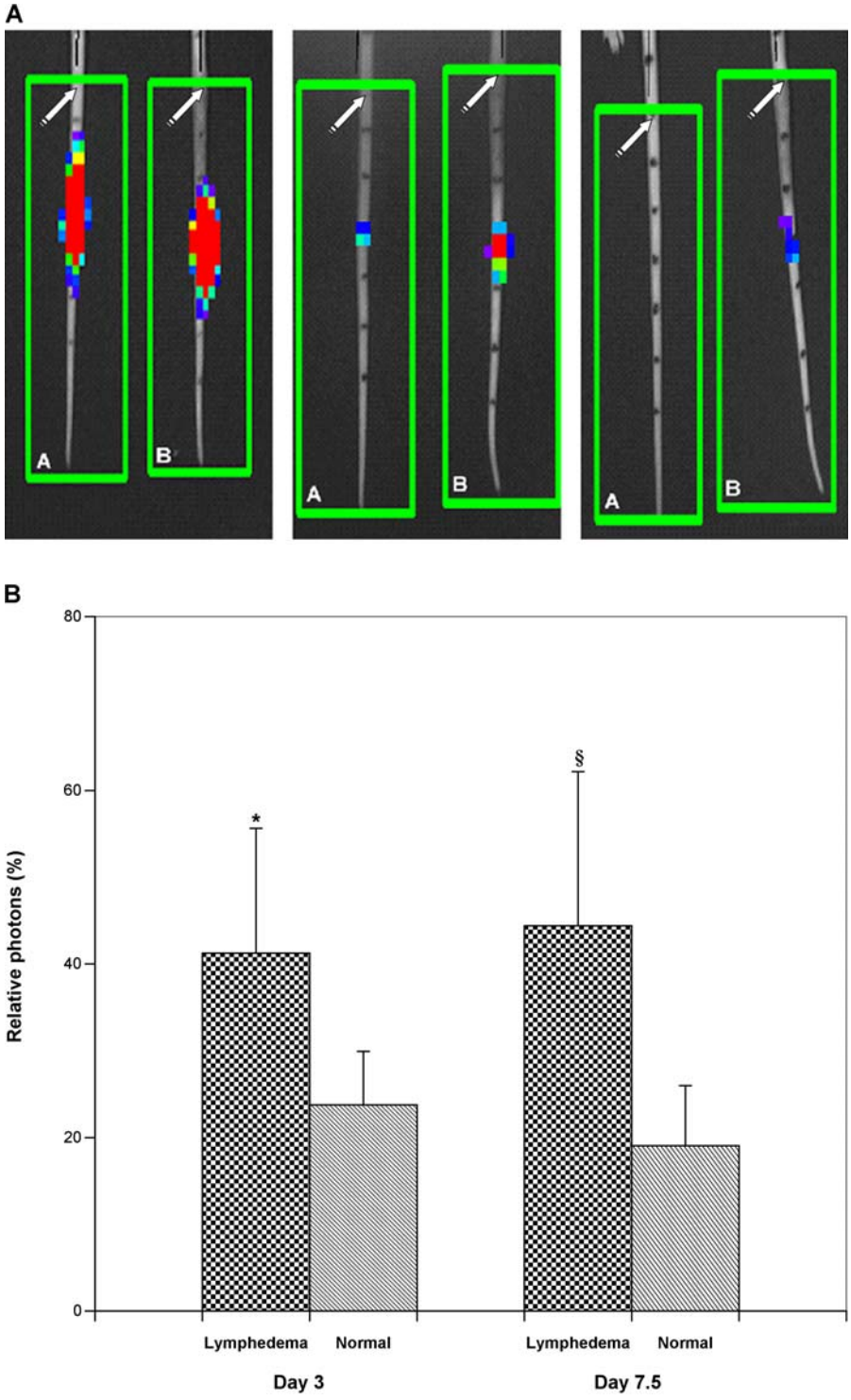

Figure 4. Dynamic Imaging of Immune Traffic in Experimental Lymphedema

(A) In vivo bioluminescence imaging of immune traffic. Bioluminescence imaging was performed at defined time points following the introduction of *luc*$^{+}$ cells. This figure contains a representative series of imaging experiments for paired normal control (A) and lymphedema (B) mice. Photon densities range from red (high) to blue (low). In general, clearance of bioluminescent immunocytes from the lymphedematous tails was delayed, but remained unimpaired in the surgical sham controls. The left panel shows a perceptible increase in photon densities in lymphedema on day 3 post-injection (post-operative day 10). Within several days, the disparity in cellular clearance is even more evident (middle panel); as late as day 17 post-injection, there is still visible bioluminescence in the lymphedematous tail, while all activity has cleared from the normal tail (right panel). The original surgical site is depicted by the white arrows. The black marks on the tail denote 8-mm vertical distances; splenocyte injection was performed 24 mm below the surgical site.

(B) Quantitative assessment of in vivo bioluminescence imaging of immune traffic. Relative photon density, expressed as a percent of the observed value on day 1, was significantly greater in lymphedema than in normal controls, both at day 3 and at day 7 post-injection (*, $p < 0.05$; §, $p < 0.02$).

DOI: 10.1371/journal.pmed.0030254.g004

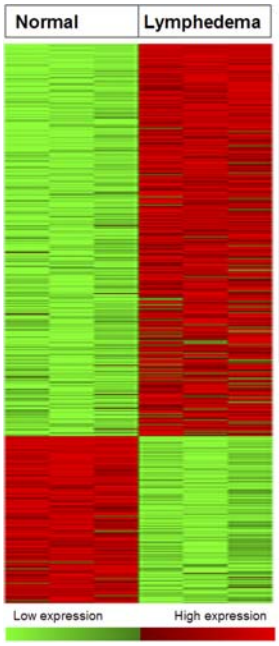

Pathway Analysis for genes up in Lymphedema vs. Normal

Annotation	Gene Category	p value
GO Molecular Function	defense/immunity protein activity	0.0000
GO Molecular Function	extracellular matrix structural constituent conferring tensile strength	0.0002
GO Molecular Function	extracellular matrix structural constituent	0.0005
GO Molecular Function	complement activity	0.0015
GO Molecular Function	structural molecule activity	0.0041
GO Biological Process	response to pest/pathogen/parasite	0.0001
GO Biological Process	immune response	0.0003
GO Biological Process	response to stress	0.0004
GO Biological Process	response to biotic stimulus	0.0004
GO Biological Process	defense response	0.0006
GO Biological Process	complement activation	0.0044
GO Biological Process	humoral immune response	0.0054
GO Cellular Component	extracellular space	0.0000
GO Cellular Component	extracellular	0.0001
GO Cellular Component	collagen	0.0004
GO Cellular Component	mitochondrion	0.0006
GO Cellular Component	cytoplasm	0.0009

Pathway Analysis for genes up in Normal vs. Lymphedema

Annotation	Gene Category	p value
GO Biological Process	lipid metabolism	0.0013
GO Biological Process	coenzyme and prosthetic group metabolism	0.0018
GO Biological Process	coenzyme and prosthetic group biosynthesis	0.0025
GO Biological Process	biosynthesis	0.0032
GO Biological Process	lipid biosynthesis	0.0039
GO Biological Process	coenzyme metabolism	0.0103

Figure 5. SAM Analysis of Microarray Data

At an FDR of 5%, SAM analysis identified 429 upregulated genes in the lymphedema state versus 183 downregulated genes. There were no statistically significant differences between normal mice and surgical control animals (SAM, FDR $<$ 25%). Enrichment analysis with the Fisher's exact test (EASE software) demonstrated several statistically significant ontologies.

DOI: 10.1371/journal.pmed.0030254.g005

(Figure 5). There were no statistically significant differences between normal mice and surgical control animals (SAM, FDR $<$ 25%). A complete list of differentially regulated genes is provided in Tables 3 and 4.

To identify important biological themes represented by genes differentially expressed in the atherosclerotic lesions, we functionally annotated the genes using GO terms. Enrichment analysis with the Fisher's exact test (EASE software) demonstrated several statistically significant ontologies (Figure 5; Tables 5 and 6), including several pathways associated with inflammation. The inflammatory processes, such as defense response, immune response, response to stress, response to pest/pathogen/parasite, and complement activation, represent both humoral immune response and innate immunity.

Further scrutiny of the list of genes whose expression is significantly altered in lymphedematous skin suggests that the disease process can be characterized by alterations within a relatively small set of functional attributes, as summarized in Table 7. These processes include acute inflammatory response, wound healing and fibrosis, angiogenesis, cytoskeletal organization, *Wnt* pathway activation, and adipogenesis.

qRT-PCR Confirms the Accuracy of Microarray Hybridization Results

Differential expression of eight representative genes from various pathways was confirmed by qRT-PCR. The genes were selected to represent the spectrum of magnitude and direction of change of lymphedematous gene expression relative to normal. The genes assayed included *calgranulin A, calgranulin B, matrix metalloproteinase 3 (MMP3), matrix metalloproteinase 14 (MMP14), myeloid differentiation primary response gene 88 (MYD88), hydroxysteroid (17-beta) dehydrogenase 2 (HADH2), cadherin 11,* and *clusterin*. Overall, the results of the two methods correlated well (Figure 6).

Discussion

In this study, we have characterized a mouse model of lymphedema using in vivo functional imaging and histopathological correlation. This model of acute, acquired lymph stagnation closely simulates the volume response, histopathology, and lymphoscintigraphic characteristics of human acquired lymphedema. LYVE-1 immunohistochemistry demonstrates that this acute impairment of lymph transport is accompanied by an increase in the number and size of microlymphatic structures in the lymphedematous cutaneous tissues.

We have also undertaken molecular characterization of the disease process through comprehensive transcriptional profiling of the murine lymphedematous tail skin. We have identified a set of genes and molecular pathways that play a role in the unique biology of this cutaneous response to lymph stasis (lymphedema). Recognition of this molecular response pattern is likely to enhance our comprehension of the pathogenesis and biology of lymphedema.

The model has been elaborated to simulate the regional, acquired lymph stagnation that can arise after trauma, surgery, and cancer therapeutics [8]. Despite apparent rapid healing of the external cutaneous wound, the model features a stable, persistent edematous increase in the volume of the tail, accompanied by a profound inflammatory response; neither edema nor inflammation is seen in surgical controls.

The cutaneous inflammatory response observed in this model replicates clinical descriptions of human acquired lymphedema, where there is frequently evidence of concom-

Table 3. Upregulated Genes in Lymphedema versus Normal Control (SAM, FDR < 0.05)

Gene ID	Gene Symbol	LocusLink Accession ID	Gene Name	Score (*d*)[a]	Fold Change	*q*-Value (%)
AV020023	*S100a9*	20202	*S100 calcium binding protein A9 (calgranulin B)*	17.47	21.5	0.91
AV171621	*Stfa3*	20863	*stefin A3*	14.55	4.3	0.91
AV038429	*Rarres2*	71660	*Mus musculus,* similar to RIKEN cDNA 0610007L05 gene, clone MGC:18838 IMAGE:4212222, mRNA, complete cds	11.98	2.9	0.91
BG072297	*Fcer1g*	14127	*Fc receptor, IgE, high affinity I, gamma polypeptide*	11.02	4.2	0.91
AA139015	*B2m*	12010	*beta-2 microglobulin*	10.86	3.9	0.91
AV034788			*cytotoxic T lymphocyte-associated protein 2 alpha*	10.81	4.5	0.91
432238			EST	10.42	3.3	0.91
AV171866	*Stfa1*	20861	ESTs, highly similar to CTY3 mouse *stefin 3 (Mus musculus)*	10.04	4.6	0.91
AV068500	*Lgals2*	107753	*lysozyme*	10.02	4.6	0.91
AA003942	*Tnc*	21923; 402769	*tenascin C*	9.21	7.8	0.91
AV109517	*Cyba*	13057	*cytochrome b-245, alpha polypeptide*	8.91	2.6	0.91
W48195	*1500040F11Rik*	22272	RIKEN cDNA 1500040F11 gene	8.80	1.8	0.91
43822			EST	8.68	2.1	0.91
AW547306	*C1qg*	12262	*complement component 1, q subcomponent, c polypeptide*	8.38	2.6	0.91
AV083964			*heme oxygenase (decyling) 1*	8.12	1.6	0.91
BG073325			EST	8.02	1.3	0.91
AV094691			*ubiquitin-conjugating enzyme E2 variant 1*	8.01	1.5	0.91
AV114351	*Rbp1*	19659	*retinol binding protein 1, cellular*	7.66	2.5	0.91
BG063011	*Ctla2a*	13024; 13025	*cytotoxic T lymphocyte-associated protein 2 alpha*	7.54	4.0	0.91
AV069980	*B2m*	12010	*beta-2 microglobulin*	7.47	3.2	0.91
AV133727	*Ssr4*	20832	*signal sequence receptor, delta*	7.04	1.4	0.91
431201			EST	6.84	2.7	0.91
411130			EST	6.83	2.0	0.91
AV09442			EST, weakly similar to RL 15 rat *60S ribosomal protein L15 (Rattus norvegicus)*	6.72	1.7	0.91
AV068190	*Ndufa6*	67130	*M. musculus,* similar to hypothetical protein MGC3178, clone MGC:28887 IMAGE:4911455, mRNA, complete cds	6.58	2.4	0.91
AI118893	*S100a8*	20201	EST	6.57	16.0	0.91
AW550933			EST, weakly similar to PRP3 mouse *proline-rich protein MP-3 (M. musculus)*	6.57	1.3	0.91
AV094499	*Isyna1*	71780	RIKEN cDNA 1300017C10 gene	6.49	1.6	0.91
AV060165			EST	6.37	3.9	0.91
AV066072	*Ifitm3*	66141	RIKEN cDNA 1110004C05 gene	6.35	2.1	0.91
432539			EST	6.22	3.8	0.91
AV037118	*B2m*	12010	*beta-2 microglobulin*	6.14	3.0	0.91
AV028863			*ferritin heavy chain*	6.06	2.0	0.91
AV035363	*Prg1*	19073	*proteoglycan, secretory granule*	5.98	3.7	0.91
AV013352	*1810009M01Rik*	65963	RIKEN cDNA 1810009M01 gene	5.94	2.3	0.91
AV054688	*Muc1*	17829	EST	5.93	1.7	0.91
412016			EST	5.86	3.6	0.91
411315			EST	5.84	1.8	0.91
412595			EST	5.82	1.4	0.91
AV061443	*Ifngr1*	15979	*interferon gamma receptor*	5.81	2.0	0.91
BG072156	*Ifitm3*	66141	RIKEN cDNA 1110004C05 gene	5.78	3.7	0.91
413077			EST	5.73	1.7	0.91
AV035765			EST	5.72	4.5	0.91
AA177689	*Mrg2*	17537	*myeloid ecotropic viral integration site-related gene 2*	5.71	1.6	0.91
AA162879			*stromal cell-derived factor 1*	5.70	2.4	0.91
AV052140	*Cxcl12*	20315	*stromal cell-derived factor 1*	5.63	2.0	0.91
AA087526	*Rbp1*	19659	*retinol binding protein 1, cellular*	5.59	2.9	0.91
AV109528			*myosin light chain, alkali, nonmuscle*	5.57	1.7	0.91
AV108847	*Gnl2*	230737	*M. musculus,* similar to *nucleolar GTPase,* clone MGC: 7863 IMAGE: 3501393, mRNA complete cds	5.54	2.3	0.91
BG070106	*Lcn2*	16819	*lipocalin 2*	5.47	6.1	0.91
431107			EST	5.41	2.6	1.08
BG073227	*Fbln2*	14115	*fibulin 2*	5.41	2.0	1.08
AA072722	*Fcer1g*	14127	*Fc receptor, IgE, high affinity I, gamma polypeptide*	5.35	3.0	1.08
412394			EST	5.31	1.7	1.08
BG063844	*Lcp1*	18826	*plastin 2, L*	5.29	3.3	1.08
AV087823	*Cbr2*	12409	*carbonyl reductase 2*	5.29	1.8	1.08
413592			EST	5.28	2.4	1.08
AV036203	*Lsp1*	16985	*lymphocyte specific 1*	5.22	1.7	1.08
AV141619			RIKEN cDNA 1810037I17 gene	5.22	1.4	1.08
BG074642	*BC027309*	243371	RIKEN cDNA 0610007L05 gene	5.21	2.5	1.08
AV070323	*Ndufab1*	70316	RIKEN cDNA 2610003B19 gene	5.21	1.7	1.08
AV104403	*Ctsz*	64138	*cathepsin Z*	5.17	2.2	1.08

Table 3. Continued

Gene ID	Gene Symbol	LocusLink Accession ID	Gene Name	Score (d)[a]	Fold Change	q-Value (%)
BG068219	*Lgmn*	19141	*legumain*	5.16	2.4	1.08
AV085954			*complement component 1, q subcomponent, beta polypeptide*	5.15	3.2	1.08
AV058060	*Calm1*	12313	*calmodulin 1*	5.15	1.8	1.08
AV087404	*2310056P07Rik*	70186	RIKEN cDNA 2310056P07 gene	5.09	1.6	1.08
AV094766			*M. musculus,* similar to *aspartyl-tRNA synthetase,* clone MGC:6719 IMAGE:3586278, mRNA, complete cds	5.08	2.3	1.08
AV024220			*follistatin-like*	5.03	3.2	1.08
411275			EST	5.03	2.0	1.08
AV088911	*Sh3yl1*	24057	*S100 calcium binding protein A11 (calizzarin)*	4.97	1.6	1.08
AV109524	*Cxcl4*	56744	*platelet factor 4*	4.96	1.8	1.08
AV094436	*Uqcrc1*	22273	*ubiquinol-cytochrome c reductase core protein 1*	4.96	2.2	1.08
AI875081	*Gpx1*	14775	*glutathione peroxidase 1*	4.95	1.9	1.08
AV104473	*Ctsz*	64138	*cathepsin Z*	4.92	2.0	1.08
AV093499	*Tmsb4x*	19241	*thymosin, beta 4, X chromosome*	4.91	1.7	1.08
AV001464	*Grn*	14824	*granulin*	4.90	1.7	1.08
AV087961	*Emcn*	59308	*endomucin*	4.88	1.7	1.08
BG074570			*myosin light chain, alkali, nonmuscle*	4.83	1.5	1.08
AV113890	*Fabp5*	16592	*fatty acid binding protein 5, epidermal*	4.81	1.9	1.08
AV133965	*Esd*	13885	*esterase 10*	4.81	1.9	1.08
AV084804	*Tagln2*	21346	*M. musculus,* similar to *transgelin 2,* MGC:6300 IMAGE:2654381, mRNA,complete cds	4.80	1.6	1.08
BG071322	*Cbr2*	12409	*carbonyl reductase 2*	4.78	1.6	1.08
AI847496	*Snx5*	69178	*sorting nexin 5*	4.78	2.0	1.08
AV093793			*ribosomal protein L24*	4.76	1.4	1.08
AW556849			EST	4.73	1.5	1.08
AI841291			*spermidine/spermine N1-acetyl transferase*	4.72	1.5	1.08
411545			EST	4.70	2.7	1.08
BG073274	*Gnai2*	14678	*guanine nucleotide binding protein, alpha inhibiting 2*	4.65	1.5	1.08
AV014173	*Dnajc13*	235567	ESTs, highly similar to T00361 hypothetical protein KIAA0678 *(Homo sapiens)*	4.59	1.8	1.36
AV009300	*Col4a1*	12826	*procollagen, type IV, alpha 1*	4.54	2.0	1.36
AV010312	*Col4a2*	12827	*procollagen, type IV, alpha 2*	4.50	2.0	1.36
BG074937	*H2-D1*	14964; 14980; 14972; 497653; 15013	*histocompatiblility 2, D region locus 1*	4.49	2.1	1.36
W14193	*S100a9*	20202	*S100 calcium binding protein A9 (calgranulin B)*	4.47	14.9	1.36
AV023779	*Sssca1*	56390; 17826	*Sjogren's syndrome/scleroderma autoantigen 1 homolog (H. sapiens)*	4.47	3.7	1.36
AV086173	*Ppib*	19035	*peptidylprolyl isomerase B*	4.41	1.4	1.59
431892			EST	4.40	2.8	1.59
432647			EST	4.39	3.4	1.59
431995			EST	4.39	1.5	1.59
AV095167	*Gpx1*	14775	*glutathione peroxidase 1*	4.38	1.7	1.59
AI596034	*Ror2*	26564; 78531	*receptor tyrosine kinase-like orphan receptor 2*	4.35	1.7	1.59
411582			EST	4.34	1.3	1.59
BG067559	*Ctsc*	13032	*cathepsin C*	4.33	2.3	1.59
AV086001		209294	ESTs, highly similar to CYT3 mouse *stefin 3 (M. musculus)*	4.33	2.3	1.59
AV171061	*Cotl1*	72042	*coactosin-like protein*	4.32	1.3	1.59
BG065250	*Ctsh*	13036	*cathepsin H*	4.32	1.5	1.59
AV017041			*N-acetylneuraminate pyruvate lyase*	4.30	4.1	1.59
AV096227			*thymosin, beta 10*	4.29	2.5	1.59
411500			EST	4.28	2.7	1.59
AV106608			*glutathione peroxidase 1*	4.27	1.8	1.59
AV104166	*Alox5ap*	11690	*arachidonate 5-lipoxygenase activating protein*	4.25	2.9	1.59
AI325865	*Arpc4*	68089	*actin related protein 2/3 complex, subunit 4 (20 kDa)*	4.24	1.5	1.73
BG074171	*Stfa1*	20861	ESTs, highly similar to CYT3 mouse *stefin 3 (M. musculus)*	4.24	6.3	1.73
BG075608	*Tpi1*	21991	*triosephosphate isomerase*	4.24	1.9	1.73
AV105953			*calreticulin*	4.23	2.0	1.73
AV094913	*1110020C13Rik*	66151	RIKEN cDNA 1110020C13 gene	4.22	1.3	1.73
412705			EST	4.22	4.0	1.73
410890			EST	4.21	1.7	1.73
412501			EST	4.21	1.4	1.73
AI526714	*Gpx1*	14775	*glutathione peroxidase 1*	4.18	1.8	1.73
AV014751	*Lox*	16948	*lysyl oxidase*	4.17	2.7	1.73
BI076685			EST	4.17	1.4	1.73
AV001134	*Arhgdib*	11857	*Rho,GDP dissociation inhibitor (GDI) beta*	4.15	1.8	1.73
BG072620	*Rps6*	20104	*ribosomal protein S6*	4.14	1.3	1.73

Table 3. Continued

Gene ID	Gene Symbol	LocusLink Accession ID	Gene Name	Score (*d*)[a]	Fold Change	*q*-Value (%)
BG065930			RIKEN cDNA 3110023F10 gene	4.13	1.6	1.73
BG076357			*erythroid differentiation regulator*	4.11	2.7	1.73
AV094406			*M. musculus,* clone IMAGE:3499608, mRNA, partial cds	4.11	1.5	1.73
AW554113			EST	4.11	1.5	1.73
411855			EST	4.10	1.5	1.73
AV031220			SET translocation	4.09	1.5	1.96
BG072550	*Carhsp1*	52502	RIKEN cDNA 120011K09 gene	4.08	1.8	1.96
AV038462	*Ctla2a*	13024; 13025	*cytotoxic T lymphocyte-associated protein 2 alpha*	4.07	4.0	1.96
AV120085			*ribosomal protein S18*	4.06	1.2	1.96
AV009166			*capping protein beta 1*	4.05	1.7	1.96
412280			EST	4.04	2.9	1.96
AV111409	*Ubl5*	66177	*ubiquitin-like 5*	4.02	1.3	1.96
AV039992	*Dnajc2*	22791	*zuotin related factor 2*	4.02	1.3	1.96
AW543803			*hypoxia inducible factor 1, alpha subunit*	4.01	1.9	1.96
AW551760			*interferon induced transmembrane protein 3-like*	4.00	1.7	1.96
BG071182	*0610011I04Rik*	66058	RIKEN cDNA 0610011I04 gene	4.00	2.7	1.96
BG065327	*Aatf*	56321	*traube*	4.00	1.2	1.96
AW553642	*Cald1*	109624; 18153	*M. musculus,* similar to *caldesmon 1,* clone MGC:30319 IMAGE:5148205, mRNA, complete cds	4.00	2.1	1.96
430643			EST	4.00	3.4	1.96
432671			EST	3.98	1.8	1.96
431125			EST	3.97	2.7	1.96
AV009103			Expressed sequence AA408606	3.96	1.5	1.96
AW554082			EST	3.95	1.8	1.96
AV094414	*Slc35b1*	73836	*M. musculus,* clone MGC:31031 IMAGE:5137689, mRNA, complete cds	3.91	2.3	1.96
AV017679			*small EDRK-rich factor 2*	3.90	1.7	1.96
411766			EST	3.89	1.3	1.96
AV094647	*Ndufs8*	225887	*M. musculus,* clone MGC:37950 IMAGE:5132866, mRNA, complete cds	3.89	1.3	2.28
AV105113	*Ifitm3*	66141	RIKEN cDNA 1110004C05 gene	3.89	1.6	2.28
AF065441	*Fgfbp1*	14181	*fibroblast growth factor binding protein 1*	3.87	1.5	2.28
AV065392	*Atp6v0b*	114143	ESTs	3.87	1.4	2.28
BG063611			*lectin, galactose binding, soluble 1*	3.86	2.9	2.28
430977			EST	3.86	2.7	2.28
BG072866			*M. musculus,* clone MGC:28609 IMAGE:4218551, mRNA, complete cds	3.85	1.3	2.28
411576			EST	3.84	2.5	2.28
AV094612	*C87860*	97112	Expressed sequence C87860	3.83	1.4	2.28
BG075953	*Usp33*	170822	*Vhlh-interacting deubiquitinating enzyme 1*	3.83	1.9	2.28
AW548371			EST	3.81	1.7	2.28
432957			EST	3.81	2.1	2.28
AV109529			*ferritin heavy chain*	3.81	2.2	2.28
AV109316			*thymosin, beta 4, X chromosome*	3.81	1.7	2.28
433177			EST	3.80	1.6	2.28
413039			EST	3.80	1.8	2.28
AV070066			EST	3.78	1.5	2.28
AV294875	*Pgk1*	18655	*phosphoglycerate kinase 1*	3.78	1.7	2.28
BG072801	*S100a9*	20202	*S100 calcium binding protein A9 (calgranulin B)*	3.78	19.2	2.28
AV014493	*Zbtb17*	22642	*zinc finger protein 100*	3.78	1.6	2.28
413454			EST	3.77	4.5	2.28
BG075853	*Sepp1*	20363	*selenoprotein P, plasma 1*	3.77	2.8	2.28
AV087234	*Eef2k*	13631; 436008	Expressed sequence C86191	3.76	1.7	2.28
AV028503	*Sat1*	20229	*spermidine/spermine N1-acetyl transferase*	3.76	1.6	2.73
AV133930	*Hexa*	15211	*hexosaminidase A*	3.74	2.0	2.73
410654			EST	3.74	2.7	2.73
AV025941			*aquaporin 1*	3.74	2.0	2.73
AV050073	*S100a9*	20202	*S100 calcium binding protein A9 (calgranulin B)*	3.74	22.5	2.73
AV093600	*Atp5j2*	57423	*ATP synthase, H^+ transporting, mitochondrial F0 complex, subunit f, isoform 2*	3.73	1.6	2.73
AA408841	*Csrp1*	13007	*cystein rich protein*	3.73	1.7	2.73
AW553287			*osteoblast specific factor 2 (fasciclin I-like)*	3.72	2.1	2.73
AV043279			*cholinergic receptor, nicotinic, epsilon polypeptide*	3.71	1.6	2.73
AV134223			*fatty acid binding protein 5, epidermal*	3.70	2.2	2.73
BG063873	*Ftl1*	14325	*ferritin light chain 1*	3.70	2.4	2.73
AV134053	*Rpo1–3*	20018	*RNA polymerase 1–3 (16-kDa subunit)*	3.70	1.2	2.73
AW547223			*ribosomal protein L29*	3.68	2.5	2.73
BG064350			*actinin, alpha 1*	3.66	1.8	2.73
AV113595			*embryonic ectoderm development*	3.65	1.9	2.73
AV094967	*Cox6b1*	110323	RIKEN cDNA 2010000G05 gene	3.65	1.4	2.73

Table 3. Continued

Gene ID	Gene Symbol	LocusLink Accession ID	Gene Name	Score (*d*)[a]	Fold Change	*q*-Value (%)
AV072373			RIKEN cDNA 2510010F10 gene	3.63	2.3	2.73
AV094998	*Loxl1*	16949; 78901	*lysyl oxidase-like*	3.63	1.8	2.73
AV012373	*Tagln*	21345	*transgelin*	3.62	1.5	2.73
AA162273	*Col4a1*	12826	*procollagen, type IV, alpha 1*	3.62	3.0	2.73
BG065103	*Ly6e*	17069	*lymphocyte antigen 6 complex, locus E*	3.61	1.5	2.73
BG071626			ESTs, Moderately similar to *glyceraldehyde 3-phosphate dehydrogenase (M. musculus)*	3.60	1.5	3.17
BG074224			ESTs	3.60	1.4	3.17
AV000846	*Sod2*	20656	*superoxide dismutase 2, mitochondrial*	3.58	1.5	3.17
AV030230	*5330438D12Rik*	327824	ESTs	3.57	2.2	3.17
AA980714	*Pecam1*	18613	*platelet/endothelial cell adhesion molecule*	3.56	2.0	3.17
AV162332			RIKEN cDNA 3110001M13 gene	3.55	2.3	3.17
412441			EST	3.55	1.8	3.17
AV031080	*Ubl3*	24109	*ubiquitin-like 3*	3.55	1.9	3.17
AV030853	*D8Ertd325e*	66855	RIKEN cDNA 1100001J13 gene	3.54	1.5	3.17
AV094526	*Rps6kl1*	238323	*M. musculus,* hypothetical protein MGC11287 similar to *ribosomal protein S6 kinase*, clone MGC:28043 IMAGE:3672127, mRNA, complete cds	3.54	1.2	3.17
AV133784	*Cald1*	109624; 18153	*M. musculus,* similar to *caldesmon 1*, clone MGC:30319 IMAGE:5148205, mRNA, complete cds	3.53	1.9	3.17
C79946			Expressed sequence C79946	3.52	1.7	3.17
AA086550	*Mrg2*	17537	*myeloid ecotropic viral integration site-related gene 2*	3.52	1.6	3.17
AW550650	*Tctex1*	21648	*t-complex testis expressed 1*	3.51	1.8	3.17
AV070981			*hypoxia inducible factor 1, alpha subunit*	3.50	1.5	3.17
BG073809	*Bgn*	12111	*biglycan*	3.49	2.6	3.17
BG071407	*Mdh2*	17448	*malate dehydrogenase, mitochondrial*	3.49	1.5	3.17
AV028607	*Serpini1*	20713	*serine (or cysteine) proteinase inhibitor, clade I (neuroserpin), member 1*	3.48	1.9	3.17
AV006041	*2900073G15Rik*	67268	RIKEN cDNA 2900073G15 gene	3.48	1.6	3.17
412701			EST	3.48	1.4	3.17
AV103730	*Arpc3*	56378	*actin related protein 2/3 complex, subunit 3 (21 kDa)*	3.48	1.7	3.17
AV109544	*Map1lc3b*	67443	*microtubule-associated protein 1 light chain 3*	3.48	1.3	3.17
AV030400			*myosin light chain, alkali, nonmuscle*	3.45	1.7	3.17
432209			EST	3.45	2.0	3.17
AV114184	*H2-Bf*	14962	*histocompatibility 2, complement component factor B*	3.43	3.1	3.24
BG067257	*Clta*	12757	*clathrin, light polypeptide (Lca)*	3.41	1.4	3.24
BG070050	*Map1lc3b*	67443	*microtubule-associated protein 1 light chain 3*	3.41	1.3	3.24
AV017254	*Mpp1*	17524	*membrane protein, palmitoylated (55 kDa)*	3.40	1.9	3.24
AV093759	*Rps12*	20042	*ribosomal protein S12*	3.40	1.5	3.24
AI841252	*Tmem4*	56530	*transmembrane protein 4*	3.39	1.4	3.24
AV006536			EST	3.38	1.3	3.24
AV094757			EST	3.37	2.0	3.24
AV055121	*Sepx1*	27361	*selenoprotein R*	3.36	1.6	3.24
BG073062	*Atp5j2*	57423	*ATP synthase, H^+ transporting, mitochondrial F0 complex, subunit f, isoform 2*	3.36	1.5	3.24
AU043587	*Map17*	67182	*membrane-associated protein 17*	3.35	1.5	3.24
AV087816	*Krt1–14*	16664	*keratin complex 1, acidic, gene 14*	3.34	1.4	3.24
AV074746			*thymosin, beta 4, X chromosome*	3.34	1.7	3.24
AV087388	*0910001A06Rik*	223601	*M. musculus,* similar to hypothetical protein DKFZp566A1524, clone MGC:18989 IMAGE:4012217, mRNA, complete cds	3.33	2.1	3.24
BG065030	*Gpx1*	14775	*glutathione peroxidase 1*	3.33	1.5	3.24
BG071424	*Itm2c*	64294	*integral membrane protein 3*	3.33	1.3	3.24
AV133758		432633	*phosphoglycerate kinase 1*	3.33	2.3	3.24
BG075599	*Mpp1*	17524	*membrane protein, palmitoylated (55 kDa)*	3.31	1.4	3.24
AV094520	*Htf9c*	15547	*Hpall tiny fragments locus 9c*	3.31	1.5	3.24
BG064704			*lectin, galactose binding, soluble 1*	3.31	2.0	3.53
411696			EST	3.29	1.4	3.53
AV019210	*Eln*	13717	elastin	3.29	1.8	3.53
AV084625			*BTB (POZ) domain containing 1*	3.29	1.6	3.53
AV037171	*BC064011*	407790	ESTs, Weakly similar to NUML mouse *NADH-ubiquinone oxidoreductase MLRQ subunit (M. musculus)*	3.28	1.3	3.53
BG063257	*2510027N19Rik*	67711	RIKEN cDNA 2510027N19 gene	3.28	1.6	3.53
AV033994	*Prg1*	19073	*proteoglycan, secretory granule*	3.27	3.7	3.53
AV081086			EST	3.27	1.7	3.53
412241			EST	3.25	1.4	3.53
AV006019	*Pigq*	14755	*phosphatidylinositol glycan, class Q*	3.24	1.7	3.53
AV013830	*S100a13*	20196	*S100 calcium binding protein A13*	3.24	1.3	3.53

Table 3. Continued

Gene ID	Gene Symbol	LocusLink Accession ID	Gene Name	Score (d)[a]	Fold Change	q-Value (%)
AV015250			*DnaJ (Hsp40) homolog, subfamily B, member 5*	3.24	2.6	3.53
204387			EST	3.24	1.6	3.53
AW323058	*Hsd17b4*	15488	*CD63 antigen*	3.23	1.5	3.53
AI574416	*Tgfb2*	21808	*transforming growth factor, beta 2*	3.23	1.8	3.53
BG063870	*Actb*	11461	*actin, beta, cytoplasmic*	3.22	1.3	3.53
410751			EST	3.22	1.4	3.53
431101			EST	3.22	1.7	3.53
410791			EST	3.21	1.5	3.53
BE307724	*Psap*	19156	*prosaposin*	3.20	1.4	3.53
AV073780	*Txln*	109658	RIKEN cDNA 2600010N21 gene	3.19	1.9	3.53
AV308712			*GLI-Kruppel family member GLI*	3.19	1.4	3.53
BG072588			RIKEN cDNA 2410030A14 gene	3.19	1.4	3.53
AV074050			*retinol binding protein 1, cellular*	3.18	1.8	3.53
AV035206	*Ehhadh*	74147	RIKEN cDNA 1300002P22 gene	3.17	2.1	3.53
AV094410	*5430413I02Rik*	56742	*differential display and activated by p53*	3.17	1.3	3.53
AV171092	*Actc1*	11464	*actin, alpha, cardiac*	3.17	1.2	3.53
411087			EST	3.16	1.5	3.53
BG064536	*Kdelr2*	66913	RIKEN cDNA 1110007A14 gene	3.16	1.6	3.53
AA776162	*CACNA1B*	774	*calcium channel, voltage-dependent, L type, alpha 1B subunit*	3.15	1.6	3.73
AV162471			EST	3.15	2.1	3.73
AV041829			*thymosin, beta 10*	3.15	2.3	3.73
412704			EST	3.15	1.3	3.73
AV089281	*Col5a2*	12832	*procollagen, type V, alpha 2*	3.14	2.4	3.73
AV109643			*Niemann Pick type C2*	3.14	2.0	3.73
AI325874	*Hspe1*	15528	*heat shock 10-kDa protein 1 (chaperonin 10)*	3.13	1.5	3.73
432933			EST	3.13	1.3	3.73
BG065380	*Pkm2*	18746	*pyruvate kinase 3*	3.13	1.3	3.73
BG063305	*Atp1b1*	11931	*ATPase, Na^+/K^+ transporting, beta 1 polypeptide*	3.12	1.3	3.73
BG069782	*Hsd17b4*	15488	*CD63 antigen*	3.10	1.5	3.73
BG064917	*Tmem14c*	66154	RIKEN cDNA 1110021D01 gene	3.10	1.3	3.73
BG072879	*2610524G07Rik*	66494	*cytochrome P450, steroid inducible 3a11*	3.10	1.3	3.73
AV093637	*Pafah1b3*	18476	*platelet-activating factor acetylhydrolase, isoform 1b, alpha 1 subunit*	3.09	1.4	3.73
AV052389	*Spink4*	20731	*serine protease inhibitor, Kazal type 4*	3.09	2.6	3.73
RW:284			EST	3.08	3.7	3.73
AV094857	*2410003B16Rik*	72333	RIKEN cDNA 2410003B16 gene	3.08	1.4	3.73
411234			EST	3.08	1.9	3.73
AV156366			*glyceraldehyde 3-phosphate dehydrogenase*	3.08	1.6	3.73
41261			EST	3.08	1.8	3.73
BG066823	*Ckmt1*	12716	*creatine kinase, mitochondrial 1, ubiquitous*	3.07	1.5	3.73
AV028632			RIKEN cDNA 5530601H04 gene	3.07	1.9	3.73
AV094958	*Sec22l1*	20333	*SEC22 vesicle trafficking protein-like 1 (S. cerevisiae)*	3.07	1.4	3.73
X77585	*Txn1*	22166	*thioredoxin 1*	3.07	1.6	3.73
AV049504			EST, weakly similar to RL37 human 60S *ribosomal protein L37 (R. norvegicus)*	3.07	1.2	3.73
412915			EST	3.06	1.6	3.73
BG071240	*Cox7c*	12867; 18738	*phosphatidylinositol transfer protein*	3.06	1.3	3.73
AV088363	*Rplp2*	67186	*ribosomal protein, large P2*	3.06	1.4	3.73
AW989643			EST	3.05	1.9	3.73
AV149918	*Car2*	12349	*carbonic anhydrase 2*	3.05	2.1	3.74
AV084873	*Laptm5*	16792	*lysosomal-associated protein transmembrane 5*	3.05	1.7	3.74
BG072998			Expressed sequence AU018638	3.04	1.8	3.74
413190			EST	3.03	1.3	3.74
AA000350	*Fbn1*	14118	*fibrilin 1*	3.02	1.6	3.74
BG075073	*Tmsb4x*	19241	*thymosin, beta 4, X chromosome*	3.02	1.7	3.74
AA693053	*Ptpn2*	19255	*protein tyrosine phosphatase, non-receptor type 2*	3.02	1.5	3.74
AV035959	*Rps21*	66481	RIKEN cDNA 2410030A14 gene	3.02	1.3	3.74
BG069532	*Npc2*	67963	*Niemann Pick type C2*	3.01	1.4	3.74
AV083728	*Npc2*	67963	*Niemann Pick type C2*	3.01	1.4	3.74
AA410137			EST	3.00	1.3	3.74
AV082005	*0610040D20Rik*	66070	RIKEN cDNA 0610040D20 gene	3.00	1.5	3.74
AV103733	*Emp3*	13732	*epithelial membrane protein 3*	3.00	1.4	3.74
BG063700	*Sri*	109552	RIKEN cDNA 2210417O06 gene	2.99	1.5	3.74
AA608500	*S100a6*	20200	*S100 calcium binding protein A6 (calcyclin)*	2.99	1.6	3.74
AI836995		432684	*nascent polypeptide-associated complex alpha polypeptide*	2.99	1.3	3.74
431042			EST	2.99	1.6	3.74
AV094984	*Aldoa*	11674	*aldolase 1, A isoform*	2.99	1.6	3.74

Table 3. Continued

Gene ID	Gene Symbol	LocusLink Accession ID	Gene Name	Score (*d*)[a]	Fold Change	*q*-Value (%)
AV057697	*Fbxo44*	230903	Expressed sequence AV001623	2.98	1.3	3.74
AV110745			*uncoupling protein 2, mitochondrial*	2.98	1.5	3.74
AV025885	*Cald1*	109624; 18153	*M. musculus,* similar to *caldesmon 1,* clone MGC:30319 IMAGE:5148205, mRNA, complete cds	2.98	3.1	3.74
BG070959	*Ralbp1*	19765	*Ral-interacting protein 1*	2.98	1.4	3.74
AV166088	*Zyx*	22793	*zyxin*	2.96	1.6	3.74
AV061097	*Selk*	80795	*heat shock 30-kDa protein*	2.96	1.3	3.74
AV031183			*cytochrome c oxidase, subunit Vb*	2.96	1.4	3.74
AI325844	*Prg1*	19073	*proteoglycan, secretory granule*	2.96	2.6	3.74
BG076355	*Stat3*	20848	*signal transducer and activator of transcription 3*	2.95	1.3	3.74
AV140511	*Cox7a2l*	20463	*cytochrome c oxidase subunit VIIa polypeptide 2-like*	2.95	1.2	3.74
AV078179			*selenoprotein W, muscle 1*	2.95	1.7	3.74
AV086834			*BCL2/adenovirus E1B 19-kDa interacting protein 1, NIP3*	2.94	1.7	3.74
AW550270	*Tnc*	21923; 402769	*tenascin C*	2.93	5.2	3.74
AV109501			*M. musculus,* similar to *spondin 1a,* clone MGC:18859 IMAGE:4221758, mRNA, complete cds	2.93	1.7	3.74
AV103910	*Rab11a*	53869	*RAB11a, member RAS oncogene family*	2.93	1.4	3.74
411848			EST	2.93	1.6	3.74
AV094787	*Mrpl1*	94061	*mitochondrial ribosomal protein L1*	2.92	1.6	4.03
410746			EST	2.92	1.8	4.03
BG072740	*Arpc3*	56378	*actin related protein 2/3 complex, subunit 3 (21 kDa)*	2.92	1.6	4.03
AA261240	*Sox18*	20672	*SRY-box containing gene 18*	2.92	1.8	4.03
410959			EST	2.91	1.5	4.03
BG064603	*Rshl2*	66832	*ribosomal protein L41*	2.91	1.4	4.03
431066			EST	2.90	1.2	4.03
432500			EST	2.90	1.4	4.03
AV109648	*Rbbp4*	19646	*retinoblastoma binding protein 4*	2.90	2.0	4.03
BG073560	*Cfl1*	12631	*cofilin 1, non-muscle*	2.89	1.7	4.03
AV133972	*Hnrpa1*	15382	*heterogeneous nuclear ribonucleoprotein A1*	2.89	1.8	4.03
411828			EST	2.88	1.2	4.03
AV086965			*calmodulin 1*	2.88	1.5	4.03
AV095050	*Hspa8*	15481	*heat shock 70-kDa protein 8*	2.87	1.5	4.03
AV094992			*procollagen, type IX, alpha 3*	2.87	1.6	4.03
BG066918	*Timm8b*	30057	*translocase of inner mitochondrial membrane 8 homolog b (Saccharomyces cerevisiae)*	2.87	1.5	4.03
AV108774	*Prcp*	72461	RIKEN cDNA 2510048K03 gene	2.86	2.4	4.03
BG074443	*Lgals7*	16858	*lectin, galactose binding, soluble 7*	2.86	1.3	4.03
AV104097			*basigin*	2.86	1.7	4.03
BG063004	*Lgals1*	16852	*lectin, galactose binding, soluble 1*	2.85	2.5	4.03
AV105178			ESTs	2.85	1.6	4.03
AV142972			EST	2.85	1.6	4.03
AV029181	*Syt4*	20983	*synaptotagmin 4*	2.84	2.8	4.03
BG072227	*Litaf*	56722	*LPS-induced TNF-alpha factor*	2.84	1.3	4.03
BG075934	*Taldo1*	21351	*transaldolase 1*	2.83	1.3	4.28
431681			EST	2.83	1.7	4.28
AV081042			*serine protease inhibitor 8*	2.83	1.3	4.28
BG063024	*Efhd2*	27984	RIKEN cDNA 2600015J22 gene	2.83	1.4	4.28
AV068926			*hypoxia inducible factor 1, alpha subunit*	2.83	1.4	4.28
BG064187	*Rps18*	20084	*ribosomal protein S18*	2.82	1.2	4.28
AV133978	*Taf6l*	225895	Similar to *TAF6-like RNA polymerase II, p300/CBP-associated factor (PCAF)-associated factor, 65 kD*	2.82	1.8	4.28
AV089437			*keratin complex 1, acidic, gene 13*	2.81	2.2	4.28
410900			EST	2.81	2.9	4.28
AV073989	*2310046G15Rik*	76453; 69404	RIKEN cDNA 2310046G15 gene	2.81	1.7	4.28
BF720949	*Nfkb1*	18033	*nuclear factor of kappa light chain gene enhancer in B cells 1, p105*	2.80	1.5	4.28
AV051965	*Siat7d*	20448	*sialyltransferase 7*	2.79	1.8	4.28
AV094533	*Ctsl*	13039	*cathepsin L*	2.79	1.3	4.28
AV130661		225307; 15382	*heterogeneous nuclear ribonucleoprotein A1*	2.79	1.7	4.28
AA080001	*Calm1*	12313	*calmodulin 1*	2.79	1.5	4.28
AV109477	*Ctsl*	13039	*cathepsin L*	2.79	1.5	4.28
AA066030	*Hspa2*	15512	*heat shock 70-kDa protein 2*	2.78	1.4	4.28
BG065539			RIKEN cDNA 3110023E09 gene	2.78	1.5	4.28
AV095469			*ribosomal protein L19*	2.78	1.3	4.28
BG071748	*Ube2s*	77891	RIKEN cDNA 6720465F12 gene	2.78	1.8	4.28
411794			EST	2.78	1.5	4.28
BG070325	*Nsep1*	22608	*nuclease sensitive element binding protein 1*	2.78	1.3	4.28

Table 3. Continued

Gene ID	Gene Symbol	LocusLink Accession ID	Gene Name	Score (*d*)[a]	Fold Change	*q*-Value (%)
AV070988	*Mtch2*	56428	*mitochondrial carrier homolog 2*	2.77	1.2	4.28
BG064794	*Ftl1*	14325	*ferritin light chain 1*	2.77	2.3	4.28
AI596209	*Ror2*	26564; 78531	*receptor tyrosine kinase-like orphan receptor 2*	2.77	1.4	4.28
AA815993	*Acta2*	11475	*actin, alpha 2, smooth muscle, aorta*	2.77	1.7	4.28
AV039554	*Dmrtb1*	56296	*proline-rich protein 13*	2.76	1.5	4.28
AV094728			*eukaryotic translation initiation factor 4E*	2.76	1.3	4.28
BG064454	*Tax1bp3*	76281	RIKEN cDNA 1300011C24 gene	2.76	1.4	4.28
AV006514	*Ifnar2*	15976	*interferon (alpha and beta) receptor 2*	2.76	1.5	4.28
AV086929			RIKEN cDNA 9430096L06 gene	2.75	1.8	4.28
BG063866			*Finkel-Biskis-Reilly murine sarcoma virus (FBR-MuSV) ubiquitously expressed (fox-derived)*	2.75	1.3	4.28
BG072299	*2210401K01Rik*	72289	*receptor (calcitonin) activity modifying protein 2*	2.75	1.4	4.28
412038			EST	2.75	1.4	4.28
BG067962	*1110020C13Rik*	66151	RIKEN cDNA 1110020C13 gene	2.75	1.4	4.28
412958			EST	2.75	1.4	4.28
AI226124	*Itgb1*	16412	*integrin beta 1 (fibronectin receptor beta)*	2.74	1.6	4.90
BG066897	*Ubl5*	66177	*ubiquitin-like 5*	2.74	1.2	4.90
AV067886			RIKEN cDNA 1810027O10 gene	2.74	1.5	4.90
AV086649	*Gmnn*	57441	*geminin*	2.73	1.7	4.90
AV023199			*selenoprotein W, muscle 1*	2.73	2.2	4.90
AV095185	*Rps21*	66481	RIKEN cDNA 2410030A14 gene	2.73	1.2	4.90
AV033362	*1500040F11Rik*	22272	RIKEN cDNA 1500040F11 gene	2.73	1.3	4.90
AW557788	*Flna*	192176	*filamin-like protein*	2.72	1.5	4.90
BG070952	*Vkorc1l1*	69568	RIKEN cDNA 2310024K08 gene	2.72	1.3	4.90
AV084361			RIKEN cDNA 1810036J22 gene	2.72	1.6	4.90
BG063730	*A4galt*	239559	ESTs	2.71	1.3	4.90
AV086045	*Cox7c*	12867; 18738	*phosphatidylinositol transfer protein*	2.71	1.5	4.90
BG063539	*Rps20*	67427	*ribosomal protein S20*	2.71	1.2	4.90
BG072985	*Rpl7*	19989	*ribosomal protein L7*	2.71	1.3	4.90
AV093845	*Atp5e*	67126	RIKEN cDNA 2410043G19 gene	2.71	1.6	4.90
BG068855	*Rhoa*	11848	*ribosomal protein L13a*	2.70	1.3	4.90
AV094701	*Pnkp*	59047	*polynucleotide kinase 3′-phosphatase*	2.69	1.3	4.90
BG072570	*Rplp2*	67186	*ribosomal protein, large P2*	2.69	1.3	4.90
AV123125	*Lgals1*	16852	*lectin, galactose binding, soluble 1*	2.69	2.9	4.90
BG072625			*ribosomal protein L19*	2.68	1.4	4.90
AV058085			EST	2.68	1.2	4.90
AV008001			ESTs	2.68	1.5	4.90
AA796822	*Siat4a*	20442	*sialyltransferase 4A (beta-galactosidase alpha-2,3-sialytransferase)*	2.68	1.8	4.90
W71612	*Rab11b*	19326	*RAB11b, member RAS oncogene family*	2.68	1.5	4.90
BG063081	*Tmsb10*	19240	*thymosin, beta 10*	2.67	2.2	4.90
AV015233			ESTs	2.67	2.8	4.90
AV061059	*Lyn*	17096; 70720	*Yamaguchi sarcoma viral (v-yes-1) oncogene homolog*	2.67	2.1	4.90
AV094452	*Dnclc1*	56455	*dynein, cytoplasmic, light chain 1*	2.66	1.5	4.90
AV171729			EST	2.66	1.3	4.90
AV094762	*0610042I15Rik*	56418	*prenylated SNARE protein*	2.66	1.2	4.90
AV111434	*Myl9*	98932	*transient receptor protein 2*	2.65	1.5	4.90
AV020423	*2900073G15Rik*	67268	RIKEN cDNA 2900073G15 gene	2.65	1.4	4.90
BG064580			ESTs	2.65	1.3	4.90
AV033259	*Hrmt1l2*	15469	*heterogeneous nuclear ribonucleoprotein methyltransferase-like 2 (S. cerevisiae)*	2.65	1.5	4.90
AV171094	*Tcf4*	21413	*transcription factor 4*	2.65	1.4	4.90
412427			EST	2.64	1.7	4.90
AV149856	*Pfn1*	18643	*profilin 1*	2.64	1.5	4.90
AV149997	*5730405M13Rik*	66627	RIKEN cDNA 5730405M13 gene	2.63	1.4	4.90
AV013452			Expressed sequence AW743884	2.63	2.4	4.90
AV071157			ESTs	2.63	1.3	4.90
AV065302			*membrane-associated protein 17*	2.63	1.3	4.90

[a]The unit *d* is the relative difference in gene expression, as defined in [53].
DOI: 10.1371/journal.pmed.0030254.t003

itant chronic inflammation, and regional immune responses are distorted [2]. Architectural changes in the skin and subcutaneous tissues are often profound [3]. Chronic lymph stasis typically stimulates an increase in the number of fibroblasts, adipocytes, and keratinocytes in the skin. Mononuclear cells (chiefly macrophages) often demarcate the chronic inflammatory response [3]. In affected tissues, there is an increase in collagen deposition, accompanied by adipose and connective tissue overgrowth in the edematous regions [26].

Table 4. Downregulated Genes in Lymphedema versus Normal Control (SAM, FDR < 0.05)

Gene ID	Gene Symbol	LocusLink Accession ID	Gene Name	Score (*d*)[a]	Fold Change	*q*-Value (%)
BG067123	*Cdh1*	12550	*cadherin 1*	−14.33	2.27	0.91
BG074458	*Dhcr24*	74754	RIKEN cDNA 2310076D10 gene	−11.37	2.17	0.91
AV008967			*ferrochelatase*	−10.96	1.62	0.91
AV068725	*Hod*	74318; 330108	RIKEN cDNA 1200015P04 gene	−9.82	1.44	0.91
AV030680	*D7Ertd743e*	233724	RIKEN cDNA 150031M19 gene	−9.42	1.53	0.91
AI841373	*Lxn*	17035	*latexin*	−8.82	1.97	0.91
BG066932	*Grcc3f*	14792	*M. musculus,* clone MGC:11670 IMAGE:3709076, mRNA, complete cds	−7.61	1.60	0.91
411579			EST	−7.55	1.89	0.91
AV087499			EST, moderately similar to A57474 *extracellular matrix protein 1 precursor (M. musculus)*	−7.48	1.41	0.91
AA607208	*Cdh1*	12550	*cadherin 1*	−7.45	1.59	0.91
AV133742			EST	−7.26	1.58	0.91
410895			EST	−7.20	1.75	0.91
AV024056	*Hal*	15109	*histindine ammonia lyase*	−7.20	1.39	0.91
410562			EST	−6.90	1.77	0.91
BG069499			RIKEN cDNA 6330408J20 gene	−6.75	1.31	0.91
AV017203			ESTs, highly similar to *afadin (R. norvegicus)*	−6.64	1.66	0.91
BG066839	*C80587*	229504	Expressed sequence C80587	−6.49	1.93	0.91
413288			EST	−6.35	2.02	0.91
AV080417	*Gsta4*	14860	*glutathione S-transferase, alpha 4*	−6.20	1.73	0.91
AV015934	*Ccnd1*	382098	*cyclin D1*	−6.15	1.51	0.91
AV135760		434233	RIKEN cDNA 2600017P15 gene	−6.08	1.37	0.91
AU040403	*Krt1–5*	16673	Expressed sequence AU040403	−6.07	1.43	0.91
BG069581	*Rhou*	69581	*ras homolog gene family, member U (M. musculus)*	−6.07	1.49	0.91
BG073053	*D10Ertd214e*	52637	*protein tyrosine phosphatase, receptor type, f polypeptide*	−5.77	1.42	1.08
AI841275	*3110006P09Rik*	68036	RIKEN cDNA 2810030L11 gene	−5.67	1.78	1.08
412117			EST	−5.67	1.37	1.08
AV088691	*Nrd1*	230598	*M. musculus,* similar to *N-arginine dibasic convertase 1*	−5.63	1.43	1.08
BG076206	*Gng3lg*	14705	*G protein gamma 3 linked gene*	−5.61	1.29	1.08
AV074612	*Cd164*	53599	*CD164 antigen*	−5.53	1.46	1.08
BG072568	*Dusp14*	56405	*dual specificity phosphatase 14*	−5.52	1.43	1.08
AV081291		68539	RIKEN cDNA 1110006I15 gene	−5.46	1.59	1.08
BG075873		67231	RIKEN cDNA 2810442O16 gene	−5.44	1.86	1.08
AA111722	*Ccnd1*	12443	*cyclin D1*	−5.42	1.54	1.08
AW552727		353049	*fatty acid synthase*	−5.36	1.71	1.08
BG072524	*Dgat2*	67800	*diacylglycerol O-acyltransferase 2*	−5.35	1.87	1.08
412975			EST	−5.25	1.42	1.36
AV081155			Expressed sequence AV228068	−5.23	1.74	1.36
BG071790	*Ppp1cc*	19047	*protein phosphatase 1, catalytic subunit, gamma isoform*	−5.21	1.87	1.36
AA725946			*keratin complex 1, acidic, gene 5*	−5.15	1.87	1.36
AV087069	*Arhu*	69581	*ras homolog gene family, member U*	−5.09	1.75	1.36
AV085989		52637	Expressed sequence AU043390	−5.06	1.69	1.36
BG071047		68036	RIKEN cDNA 3110006P09 gene	−5.03	1.29	1.36
AV006223	*Gsn*	66623	*gelsolin*	−5.03	1.81	1.36
AV106079	*Gpsn2*	106529	Expressed sequence AI173355	−5.03	1.65	1.36
AV094491		108673	RIKEN cDNA 4933411H20 gene	−4.92	1.46	1.36
AV057616	*Atp6v1d*	73834	*ATPase, H^+ transporting, lysosomal 34 kDa, V1 subunit D*	−4.92	1.46	1.36
AV084670	*Vil2*	22350	*villin 2*	−4.91	1.65	1.36
BG071281	*Lap3*	66988	*leucine aminopeptidase 3*	−4.89	1.36	1.36
AV022852		73731	RIKEN cDNA 1110001M24 gene	−4.88	1.70	1.36
AV005044	*Gltp*	56356	*glycolipid transfer protein*	−4.88	1.47	1.36
AW554387	*Sgpl1*	20397	*sphingosine phosphate lyase 1*	−4.88	2.03	1.36
BG069739	*Hmgcs1*	208715	*pre–B cell leukemia transcription factor 1*	−4.87	1.53	1.36
BG064974	*Hsd17b12*	56348	*hydroxysteroid (17-beta) dehydrogenase 12*	−4.85	1.50	1.36
AV086231	*Sprrl9*	67718	*small proline rich-like 9*	−4.83	1.75	1.59
411558			EST	−4.80	1.22	1.59
AV032378		109305	*M. musculus,* similar to hypothetical protein FLJ14466	−4.75	1.52	1.59
AV012833		105072	Expressed sequence AA407887	−4.74	1.14	1.59
AV029122	*Gpr56*	14766	*G protein-coupled receptor 56*	−4.73	1.51	1.59
BG071157	*Pcyt1a*	13026	*phosphate cytidylyltransferase 1, choline, alpha isoform*	−4.68	1.43	1.73
AV088664	*Cdh1*	12550	*cadherin 1*	−4.65	1.77	1.73
BG074432	*Egfl5*	230316	ESTs, weakly similar to *LMA1 laminin alpha-1 chain precursor (M. musculus)*	−4.65	1.64	1.73
AV074709	*Srebf1*	20787	*sterol regulatory element binding factor 1*	−4.63	1.86	1.73
AV043450	*Erbb2ip*	59079	*Erbb2 interacting protein*	−4.62	1.64	1.73
AV036580	*Gsn*	227753	*gelsolin*	−4.57	1.72	1.73
BG066848			Expressed sequence AI429612	−4.54	1.57	1.73
AV068741	*Acly*	104112	Expressed sequence AW538652	−4.49	1.57	1.96

Table 4. Continued

Gene ID	Gene Symbol	LocusLink Accession ID	Gene Name	Score (*d*)[a]	Fold Change	*q*-Value (%)
BG070160	*Rbm16*	106583; 319358	Expressed sequence AI447644	−4.48	1.35	1.96
413523			EST	−4.46	1.62	1.96
BG072270	*Tom1l2*	216810	Expressed sequence AU042072	−4.44	1.61	1.96
BG075104	*Ecm1*	13601	*extracellular matrix protein 1*	−4.43	1.53	1.96
BG076113	*1110002B05Rik*	104725	RIKEN cDNA 3110040D16 gene	−4.39	1.32	1.96
AV087190	*Gsn*	227753	*gelsolin*	−4.38	1.52	1.96
AV134202	*Mocs2*	17434	*molybdenum cofactor synthesis 2*	−4.35	1.56	2.28
BG076410			ESTs	−4.34	1.51	2.28
411478			EST	−4.32	1.44	2.28
412058			EST	−4.31	1.34	2.28
AV143646	*Rbbp6*	19647	*retinoblastoma binding protein 6*	−4.28	1.61	
BG069784	*Tcte1l*	67117	RIKEN cDNA 2310075M16 gene	−4.26	1.41	2.73
BG062974		104725	RIKEN cDNA 1110002B05 gene	−4.25	1.75	2.73
BG075415		78334	Expressed sequence AW228747	−4.25	1.44	2.73
BG064062	*Klf4*	16600	*Kruppel-like factor 4 (gut)*	−4.23	1.83	2.73
BG075520		70174	Expressed sequence AW547365	−4.18	1.26	2.73
AV020091			*M. musculus,* similar to hypothetical protein FLJ20552	−4.17	1.56	2.73
BG075034	*Hdac3*	15183	*histone deacetylase 3*	−4.15	1.39	2.73
AV057405	*Mthfd2*	17768	*methylenetetrahydrofolate dehydrogenase (NAD^+ dependent), methenyltetrahydrofolate cyclohydrolase*	−4.15	1.62	2.73
BG071256		70564	RIKEN cDNA 5730469M10 gene	−4.12	1.39	2.73
AV053048	*Sel1h*	20338	Expressed sequence AW493766	−4.10	1.49	2.73
BG063086		104725	RIKEN cDNA 1110002B05 gene	−4.10	1.53	2.73
AV086552	*Ube2g2*	22213	*ubiquitin-conjugating enzyme E2G 2*	−4.04	1.52	3.17
AV140482		230584	*M. musculus,* similar to hypothetical protein, clone MGC:6903 IMAGE:2655774	−4.03	1.32	3.17
AV085956	*Mgea5*	76055	RIKEN cDNA 2310016E22 gene	−4.00	1.46	3.17
BG063211			Expressed sequence AA408215	−3.99	1.46	3.17
AV059238			ESTs	−3.98	1.50	3.17
AV089020	*2410001H17Rik*	66990	RIKEN cDNA 2410001H17 gene	−3.95	1.42	3.17
AW551596		76783	ESTs, moderately similar to KIAA0874 protein *(H. sapiens)*	−3.95	1.44	3.17
BG063986	*Chc1*	100088	RIKEN cDNA 4931417M11 gene	−3.94	1.36	3.17
AU016967	*Slc31a1*	20529	RIKEN cDNA 4930445G01 gene	−3.94	1.43	3.17
AV057445	*Hist2h3c1*	15077	*histone gene complex 2*	−3.94	1.92	3.17
BG064592	*Dph2l2*	67728	RIKEN cDNA 9130020C19 gene	−3.93	1.64	3.17
AV086468	*2810442O16Rik*	67231	RIKEN cDNA 2810442O16 gene	−3.90	1.65	3.24
AV012729	*Srebf1*	67231	*sterol regulatory element binding factor 1*	−3.90	1.60	3.24
AV021055	*8-Sep*	20787	*septin 8*	−3.89	1.48	3.24
BG074257	*Atp6v1h*	108664	Expressed sequence AU022349	−3.89	1.28	3.24
BG063838		353049	*fatty acid synthase*	−3.88	1.79	3.24
AV012338	*1110058A*	66195	RIKEN cDNA 1110058A15 gene	−3.85	1.80	3.24
AV033310	*Ss18*		*synovial sarcoma translocation, Chromosome 18*	−3.82	1.34	3.24
AV012385	*Sprrl10*		*small proline rich-like 10*	−3.80	1.82	3.24
AV005017	*Sult4a1*	29859	*sulfotransferase family 4A, member 1*	−3.80	1.42	3.24
AV084927	*Sh3glb2*	227700	*M. musculus* SH3GLB2 mRNA, complete cds	−3.79	1.45	3.24
AV133665	*Dnajb1*	81489	*DnaJ (Hsp40) homolog, subfamily B, member 1*	−3.79	1.63	3.24
BG063266	*Gclc*	14629	*glutamate-cysteine ligase, catalytic subunit*	−3.78	1.27	3.24
BG075637	*Nf2*	18016	*neurofibromatosis 2*	−3.78	1.25	3.24
BG063956	*Etf1*	225363	*M. musculus, eukaryotic translation termination factor 1,* clone MGC:18745 IMAGE:3992883	−3.78	1.31	3.24
BG072153	*Mod1*	17436	*malic enzyme, supernatant*	−3.77	1.72	3.24
AV084064	*Atp9a*	11981; 436431	*ATPase, class II, type 9A*	−3.76	1.64	3.53
BG065176	*9130404D14Rik*	227737	*M. musculus,* clone IMAGE:4038329, mRNA, partial cds	−3.73	1.59	3.53
BG074922	*Rnf167*	70510	*ring finger protein 167*	−3.71	1.29	3.53
BG075099	*Rbbp6*	19647	*retinoblastoma binding protein 6*	−3.68	1.55	3.53
BG075709	*Nt5c3*	107569	RIKEN cDNA 2610206B05 gene	−3.67	1.49	3.53
BG072411	*Epb4.1l4b*	54357	*erythrocyte protein band 4.1-like 4b*	−3.66	1.51	3.53
AV085951	*Calm4*	80796	*calmodulin 4*	−3.65	1.30	3.53
AV041686	*Rmp*	19777	*RPB5-mediating protein*	−3.64	1.79	3.53
BG063540	*Sypl*	19027	*pantophysin*	−3.63	1.32	3.73
BG063290	*Nfe2l1*	18023	*nuclear factor, erythroid-derived 2-like 1*	−3.62	1.38	3.73
AF249870	*Perp*	64058	*p53 apoptosis effector related to Pmp22*	−3.62	1.30	3.73
AV013952	*1300007F*	67477	RIKEN cDNA 1300007F04 gene	−3.62	1.53	3.73
AV065655	*Hod*	74318; 330108	RIKEN cDNA 1200015P04 gene	−3.60	1.61	3.73
BG074645	*2210413I1*	109004	ESTs, moderately similar to T42707 hypothetical protein DKFZp586EO41.1 *(H. sapiens)*	−3.59	1.44	3.73
BG063778	*Dag1*	13138	*dystroglycan 1*	−3.58	1.30	3.73
AV015196			Expressed sequence AI195353	−3.58	1.81	3.73

Table 4. Continued

Gene ID	Gene Symbol	LocusLink Accession ID	Gene Name	Score (*d*)[a]	Fold Change	*q*-Value (%)
BG068048	*1110007A06Rik*	68477	Hypothetical protein, clone MTA.D02.090	−3.57	1.38	3.73
AV034519	*Hmgcr*	15357	*3-hydroxy-3-methylglutaryl-coenzyme A reductase*	−3.54	1.48	3.73
AU020667	*Uchl3*	50933	*ubiquitin carboxyl-terminal esterase L3 (ubiquitin thiolesterase)*	−3.54	1.31	3.73
AV094982	*Rgs19ip1*	67903	*regulator of G-protein signaling 19 interacting protein 1*	−3.54	1.50	3.73
AA106674	*Ltbp4*	108075	RIKEN cDNA 2310046A13 gene	−3.53	1.50	3.73
BG070746	*1110067D22Rik*	216551	RIKEN cDNA 1110067D22 gene	−3.51	1.48	3.74
BG064041	*0610011N22Rik*	67433	RIKEN cDNA 0610011N22 gene	−3.49	1.34	3.74
AV049386	*0610039C*	66853	RIKEN cDNA 0610039C21 gene	−3.49	1.44	3.74
AI840878	*Hod*	74318; 330108	RIKEN cDNA 1200015P04 gene	−3.49	1.54	3.74
AV105934	*Sphk1*	20698	*sphingosine kinase 1*	−3.47	1.68	3.74
AV085893	*D10Ertd21*	52637	Expressed sequence AU043990	−3.47	1.62	3.74
AA118482	*Edg4*	53978	*endothelial differentiation, lysophosphatidic acid G-protein-coupled receptor 4*	−3.45	1.25	3.74
BG063967	*9130207N01*	212684	*M. musculus,* clone MGC:7094 IMAGE:3157493, mRNA, complete cds	−3.44	1.48	3.74
AV031353			*M. musculus,* similar to *phosphatidylserine decarboxylase,* clone MGC:7133 IMAGE:3158145,	−3.44	1.70	3.74
AV162240	*Irf3*	54131	*interferon regulatory factor 3*	−3.43	1.24	4.03
AV162274	*3110001I2*	70354	RIKEN cDNA 3110001I20 gene	−3.42	1.92	4.03
BG072974	*Neo1*	18007	ESTs	−3.40	1.53	4.03
AV005287	*Scamp2*	24044	*secretory carrier membrane protein 2*	−3.37	1.19	4.03
AV089034			Expressed sequence AI316859	−3.37	1.41	4.03
BG069319	*Baz2a*	116848	Expressed sequence AA415431	−3.37	1.61	4.03
AV087585	*Noc4*	18117	*neighbor of Cox4*	−3.36	1.35	4.03
AA863549	*Notch1*	18128	*Notch gene homolog 1 (Drosophila)*	−3.36	2.07	4.03
BG075813	*Hipk1*	15257	*homeodomain interacting protein kinase 1*	−3.36	1.38	4.03
BG075318	*3100002M*	69276	RIKEN cDNA 4933429H19 gene	−3.35	1.29	4.03
AV024434	*1200003E16Rik*	66860	RIKEN cDNA 1200003E16 gene	−3.35	1.66	4.03
BG074608	*1110003H*	68561	RIKEN cDNA 1300009F09 gene	−3.34	1.41	4.03
AV084667	*Tuft1*	22156	*tuftelin 1*	−3.33	1.56	4.03
AV087829	*Clic3*	69454	*chloride intracellular channel 3*	−3.33	1.72	4.03
BG063343	*Dhcr7*	13360	*7-dehydrocholesterol reductase*	−3.33	1.65	4.03
AV052668	*1810018L0*	70380	RIKEN cDNA 1810018L05 gene	−3.32	1.51	4.03
AI194827	*Osbpl1a*	64291	*oxysterol binding protein-like 1A*	−3.31	1.80	4.03
410847			EST	−3.31	1.41	4.28
AV093444	*Golga7*	57437; 71655	*hypothetical protein, MNCb-1213*	−3.29	1.25	4.28
BG076201	*Vil2*	22350	*villin 2*	−3.29	1.29	4.28
AV021431	*Mkrn1*	54484	ESTs	−3.29	1.39	4.28
BG072487	*3110018K*	73122	RIKEN cDNA 3110118K12 gene	−3.27	1.37	4.28
AV084649	*Ldb1*	16825	*LIM domain binding 1*	−3.27	1.36	4.28
AV081983	*Hop*	74318	RIKEN cDNA 1200015P04 gene	−3.27	1.51	4.28
AV055811	*Ugalt2*	110172	*UDP-galactose translocator 2*	−3.26	1.22	4.28
BG075832	*Ccnd2*	12444	*cyclin D2*	−3.26	1.50	4.28
413170			EST	−3.24	1.38	4.28
BG070048	*Hipk1*	15257	*homeodomain interacting protein kinase 1*	−3.24	1.30	4.28
AV040013	*Tes3*	114893	Expressed sequence C85469	−3.23	1.36	4.28
AV084288	*Sprrl2*	73722	*small proline rich-like 2*	−3.22	1.60	4.90
AV093474	*1300009F*	66890	RIKEN cDNA 1300009F09 gene	−3.19	1.35	4.90
AV149993	*Rnf167*	70510	*ring finger protein 167*	−3.19	1.49	4.90
411517			EST	−3.18	1.36	4.90
BG075876	*Atp9a*	11981; 436431	*ATPase, class II, type 9A*	−3.18	1.31	4.90
BG075368	*LOC21616*	216169	*M. musculus,* similar to CGI-67 protein, clone MGC:11699 IMAGE:3964094, mRNA, complete cds	−3.17	1.48	4.90
410554			EST	−3.17	1.43	4.90
BG071335	*5730469M*	70564	RIKEN cDNA 5730469M10 gene	−3.16	1.54	4.90
BG074934	*2810037C*	67211	RIKEN cDNA 2810037C14 gene	−3.16	1.42	4.90
BG063413			*CD2 antigen (cytoplasmic tail) binding protein 2*	−3.14	1.32	4.90

[a]The unit *d* is the relative difference in gene expression, as defined in [53].
DOI: 10.1371/journal.pmed.0030254.t004

Table 5. Pathway Analysis for Upregulated Genes in Lymphedema versus Normal Control (SAM, FDR < 0.05)

System	Gene Category	List Hits	List Total	Population Hits	Population Total	*p*-Value	Unigene Clusters
GO Biological Process	Response to pest/pathogen/parasite	11	101	252	10,778	0.0001	MM.163; MM.2128; MM.22673; MM.23905; MM.249934; MM.2570; MM.3453; MM.45436; MM.465; MM.653; MM.8655
	Immune response	14	101	451	10,778	0.0003	MM.141021; MM.163; MM.1776; MM.2128; MM.22673; MM.23905; MM.249934; MM.2570; MM.3453; MM.45436; MM.465; MM.549; MM.653; MM.8655
	Response to stress	15	101	538	10,778	0.0004	MM.1090; MM.12145; MM.163; MM.203; MM.2128; MM.22673; MM.23905; MM.249934; MM.2570; MM.29057; MM.3453; MM.45436; MM.465; MM.653; MM.8655
	Response to biotic stimulus	16	101	606	10,778	0.0004	MM.1090; MM.141021; MM.163; MM.1776; MM.2128; MM.22673; MM.23905; MM.249934; MM.2570; MM.29865; MM.3453; MM.45436; MM.465; MM.549; MM.653; MM.8655
	Defense response	15	101	553	10,778	0.0006	MM.141021; MM.163; MM.1776; MM.2128; MM.22673; MM.23905; MM.249934; MM.2570; MM.29865; MM.3453; MM.45436; MM.465; MM.549; MM.653; MM.8655
	Complement activation	4	101	36	10,778	0.0044	MM.2570; MM.3453; MM.653; MM.8655
	Humoral immune response	5	101	76	10,778	0.0054	MM.2570; MM.3453; MM.45436; MM.653; MM.8655
	Humoral defense mechanism (sensu Vertebrata)	4	101	42	10,778	0.0068	MM.2570; MM.3453; MM.653; MM.8655
	Nicotinamide metabolism	3	101	14	10,778	0.0072	MM.21454; MM.29182; MM.4222
	Pyridine nucleotide metabolism	3	101	15	10,778	0.0083	MM.21454; MM.29182; MM.4222
	Oxidoreduction coenzyme metabolism	3	101	17	10,778	0.0106	MM.21454; MM.29182; MM.4222
	Carbohydrate metabolism	8	101	304	10,778	0.0228	MM.14825; MM.180337; MM.21743; MM.2284; MM.29182; MM.29357; MM.4222; MM.45436
	Water-soluble vitamin metabolism	3	101	30	10,778	0.0313	MM.21454; MM.29182; MM.4222
	Response to external stimulus	17	101	1,070	10,778	0.0370	MM.1090; MM.141021; MM.163; MM.1776; MM.196464; MM.2128; MM.22673; MM.23905; MM.249934; MM.2570; MM.29865; MM.3453; MM.45436; MM.465; MM.549; MM.653; MM.8655
	Main pathways of carbohydrate metabolism	4	101	80	10,778	0.0381	MM.14825; MM.21743; MM.29182; MM.4222
GO Cellular Component	Extracellular space	42	112	2,198	10,767	0.0000	MM.10299; MM.10406; MM.141312; MM.163; MM.17185; MM.172; MM.181021; MM.182434; MM.18625; MM.19844; MM.2128; MM.21767; MM.22194; MM.22673; MM.22699; MM.2277; MM.23905; MM.2412; MM.2570; MM.2608; MM.27343; MM.28231; MM.28484; MM.29599; MM.29778; MM.3014; MM.3453; MM.36661; MM.41560; MM.43831; MM.45436; MM.46053; MM.465; MM.549; MM.653; MM.7091; MM.7281; MM.738; MM.8655; MM.86922; MM.9537; MM.980
	Collagen	5	112	34	10,767	0.0004	MM.10299; MM.141312; MM.181021; MM.7281; MM.738
	Mitochondrion	17	112	618	10,767	0.0006	MM.10406; MM.1090; MM.14825; MM.18625; MM.20801; MM.21454; MM.215667; MM.2159; MM.21743; MM.24108; MM.251621; MM.29057; MM.29599; MM.30072; MM.3014; MM.400; MM.8688
	Cytoplasm	55	112	3,659	10,767	0.0009	MM.10406; MM.1090; MM.121878; MM.141741; MM.142095; MM.142729; MM.14825; MM.153911; MM.17185; MM.181880; MM.18625; MM.196484; MM.20801; MM.21454; MM.215667; MM.2159; MM.21743; MM.2241; MM.2277; MM.2284; MM.24108; MM.2412; MM.24608; MM.249934; MM.251621; MM.2551; MM.260084; MM.2734; MM.28100; MM.28622; MM.28693; MM.29057; MM.29182; MM.29357; MM.29599; MM.29997; MM.30072; MM.3014; MM.34246; MM.3532; MM.3746; MM.38055; MM.400; MM.4024; MM.41560; MM.4222; MM.42790; MM.6523; MM.686; MM.7091; MM.741; MM.757; MM.831; MM.83909; MM.8688
	Mitochondrial matrix	4	112	64	10,767	0.0282	MM.14825; MM.21743; MM.24108; MM.29599
	Collagen type V	2	112	3	10,767	0.0306	MM.10299; MM.7281

Table 5. Continued

System	Gene Category	List Hits	List Total	Population Hits	Population Total	*p*-Value	Unigene Clusters
	Mitochondrial membrane	6	112	174	10,767	0.0339	MM.10406; MM.18625; MM.251621; MM.29057; MM.3014; MM.400
	Mitochondrial electron transport chain	3	112	32	10,767	0.0427	MM.251621; MM.3014; MM.400
GO Molecular Function	Defense/immunity protein activity	9	109	129	11,303	0.0000	MM.141741; MM.1776; MM.2570; MM.28231; MM.3453; MM.45436; MM.465; MM.653; MM.8655
	Extracellular matrix structural	6	109	68	11,303	0.0005	MM.10299; MM.141312; MM.181021; MM.29865; MM.7281; MM.738
	Complement activity	4	109	24	11,303	0.0015	MM.2570; MM.3453; MM.653; MM.8655
	Structural molecule activity	14	109	591	11,303	0.0041	MM.10299; MM.107869; MM.121878; MM.141312; MM.181021; MM.24108; MM.29057; MM.29599; MM.29865; MM.29982; MM.42790; MM.686; MM.7281; MM.738
	Actin binding	7	109	179	11,303	0.0073	MM.121878; MM.141741; MM.142729; MM.153911; MM.30059; MM.3532; MM.4024
	Heparin binding	4	109	47	11,303	0.0101	MM.182434; MM.23905; MM.46053; MM.7281
	Isomerase activity	5	109	100	11,303	0.0153	MM.2412; MM.28100; MM.28622; MM.29357; MM.4222
	Antimicrobial peptide activity	3	109	22	11,303	0.0184	MM.141741; MM.28231; MM.45436
	Glycosaminoglycan binding	4	109	59	11,303	0.0187	MM.182434; MM.23905; MM.46053; MM.7281
	Structural constituent of muscle	3	109	28	11,303	0.0291	MM.121878; MM.29057; MM.686
	Electron transporter activity	6	109	181	11,303	0.0296	MM.10406; MM.21062; MM.28622; MM.30072; MM.38746; MM8688
	Cytoskeletal protein binding	7	109	248	11,303	0.0315	MM.121878; MM.141741; MM.142729; MM.153911; MM.30059; MM.3532; MM.4024
	Hydrolase activity, acting on glycosyl bonds	4	109	82	11,303	0.0436	MM.180337; MM.203; MM.2284; MM.45436
	Oxidoreductase activity, acting on the CH-OH group of donors, NAD, or NADP as acceptor	4	109	86	11,303	0.0491	MM.14825; MM.21454; MM.21743; MM.28100

DOI: 10.1371/journal.pmed.0030254.t005

In the current study, the molecular expression profile of lymphedema, observed in parallel with the histopathology and the dynamic immune traffic imaging, suggests that the deranged immune traffic plays at least a passive, if not an active, role in the pathogenesis of the disorder. In normal immune traffic, mononuclear phagocytes and lymphocytes from the tissues enter the afferent lymph vessels and the lymph nodes to elicit primary immune responses before reentering the vasculature [5]. It is conceivable that, in chronic lymphedema, the impairment of lymphocyte and Langerhans cell trafficking from skin to regional lymph nodes leads to inefficient clearance of foreign antigens, and provides the substrate for chronic inflammatory changes [4]. The complex biology of lymphedema is still quite poorly understood. Although it has been conjectured that inflammation may indeed trigger various forms of lymphangiogenesis [27,28], the physiological sensors, signaling mechanisms, and cause-and-effect relationships that initiate post-natal lymphangiogenesis remain to be elucidated.

Transcriptional profiling has been utilized to identify genes activated in disease states and to refine targets for molecular therapy. Microarray technology has been applied to the elucidation of endothelial biology in health and disease [9,29], as well as to the investigation of gene expression patterns in cutaneous diseases [30] and in a wide array of non-neoplastic diseases that entail inflammatory or immune responses [31]. This approach is particularly attractive for the problem of acquired lymphedema, where the heterogeneous cellular composition of the tissues exposed to lymph stagnation presupposes a very complex, interdependent pattern of gene expression. While the characteristic expression profiles of isolated lymphatic endothelia have previously been studied [6,7], the current investigation represents the first in-depth molecular examination of the end-organ response to lymph stagnation. Despite the heterogeneous nature of the cellular material under investigation, the approach of high-throughput transcriptional profiling and statistical gene ontology analysis has disclosed discernable patterns of gene expression that appear to be representative of the disorder under scrutiny.

Transcriptional profiling can provide not only a gene-by-gene view of physiological alterations in a diseased state, but also a statistically rigorous identification of the biological processes that are induced or repressed in disease. This provides a much broader and more comprehensive view of the disease process as a whole than does a simple gene list, making generation of hypotheses about mechanisms more informed. Based on GO functional annotations for each gene on the array [32], we used Fisher's exact test statistical analysis to identify functional processes that are significantly induced and repressed in this disease model (Table 7). The results of this analysis were quite interesting, illustrating that whole panels of genes involved in the immune response, stress response, and complement activation are induced in lymphedema when compared to controls. Among the most interesting of the upregulated genes involved in these processes are many encoding proteins that reflect the inflammatory process. Calgranulin B, highly upregulated in this experimental model, belongs to a family of small calcium-binding proteins that are highly expressed in neutrophil and monocyte cytosol. These molecules are found at high levels in the extracellular milieu during inflammatory conditions [33].

Table 6. Pathway Analysis for Downregulated Genes in Lymphedema versus Normal Control (SAM, FDR < 0.05)

System	Gene Category	List Hits	List Total	Population Hits	Population Total	*p*-Value	Unigene Clusters
GO Biological Process	Lipid metabolism	8	47	394	10,778	0.001	MM.180189; MM.200373; MM.209300; MM.22505; MM.259976; MM.3195; MM.4141; MM.61526
	Coenzyme and prosthetic group metabolism	5	47	123	10,078	0.002	MM.19027; MM.27082; MM.30206; MM.61526; MM.6743
	Biosynthesis	11	47	874	10,078	0.003	MM.180189; MM.19027; MM.209300; MM.22505; MM.23951; MM.27082; MM.30206; MM.3845; MM.4141; MM.61526; MM.6743
	Lipid biosynthesis	5	47	152	10,778	0.004	MM.180189; MM.209300; MM.22505; MM.4141; MM.61526
	Coenzyme metabolism	4	47	106	10,778	0.010	MM.19027; MM.27082; MM.30206; MM.61526
	Steroid biosynthesis	3	47	58	10,778	0.025	MM.22505; MM.4141; MM.61526
	Metabolism	31	47	5,384	10,778	0.026	MM.10288; MM.158107; MM.180189; MM.181852; MM.19027; MM.200373; MM.202360; MM.20521; MM.20827; MM.209300; MM.220922; MM.22505; MM.23784; MM.23951; MM.2478; MM.259976; MM.26973; MM.27082; MM.27227; MM.29352; MM.30206; MM.3195; MM.34173; MM.35605; MM.3845; MM.4141; MM.42249; MM.5831; MM.61526; MM.6743; MM.9745
	Physiological process	42	47	8,273	10,778	0.028	MM.10288; MM.158107; MM.180189; MM.181852; MM.19027; MM.200373; MM.202360; MM.20521; MM.20827; MM.209300; MM.21109; MM.218875; MM.220922; MM.221298; MM.22505; MM.23784; MM.23951; MM.2478; MM.259976; MM.2632; MM.26973; MM.27082; MM.27227; MM.29352; MM.29802; MM.30195; MM.30206; MM.3195; MM.34173; MM.3433; MM.35605; MM.3845; MM.38868; MM.4141; MM.42249; MM.4480; MM.46716; MM.5181; MM.5831; MM.61526; MM.6743; MM.9745
	Macromolecule biosynthesis	8	47	731	10,778	0.034	MM.180189; MM.209300; MM.22505; MM.27082; MM.30206; MM.3845; MM.4141; MM.61526
GO Molecular Function	Catalytic activity	25	47	4,007	11,303	0.015	MM.10288; MM.158107; MM.180189; MM.200373; MM.200924; MM.202360; MM.20521; MM.20827; MM.209300; MM.22505; MM.23784; MM.23951; MM.2478; MM.2632; MM.27082; MM.27227; MM.29352; MM.29802; MM.29998; MM.30206; MM.3195; MM.42249; MM.5831; MM.61526; MM.9745

DOI: 10.1371/journal.pmed.0030254.t006

Calgranulins are potent stimulators of neutrophils and likely are involved in neutrophil migration to inflammatory sites. The levels of several of these proteins are markedly elevated in psoriasis, among other conditions [34]. Tenascin C is strongly induced by various pro- and anti-inflammatory cytokines, and its de novo expression is a reliable molecular marker for acute inflammation [35]. Peptidylprolyl isomerase B, also known as cyclophilin B, induces chemotaxis and integrin-mediated adhesion of T cells to the extracellular matrix in vitro [36]. Basigin is also involved in inflammatory processes and is proposed to be a receptor of cyclophilin A. Stromal cell-derived factor 1, also known as CXCL12, is a highly efficacious lymphocyte chemoattractant [37]. Platelet factor 4, also known as CXCL4, is a strong chemoattractant for neutrophils and fibroblasts. In addition to its putative role in inflammation, it has been implicated in the pathogenesis of atopic dermatitis. Upregulation of arachidonate 5-lipoxygenase activating protein suggests a role for leukotrienes in this acute inflammatory response; glutathione peroxidase may play an ancillary role. CD63 antigen can be interpreted as a marker of basophil activation and of degranulated neutrophils and monocytes. Legumain, an asparaginyl endopeptidase central to Class II major histocompatiblity complex presentation of microbial antigens, is a potential molecular marker of macrophage differentiation and function [38]. Follistatin is an activin antagonist implicated in wound repair; activin is an important participant in inflammation, repair, and cytoprotection in various organs, but its induction is restricted to certain types of inflammation and its release is dependent upon the inflammatory setting [39]. Nuclear factor kappa B is a transcription factor critical to the expression of a variety of chronic inflammatory disease states. The downregulation of gelsolin in this model is notable, inasmuch as hemostatic, inflammatory, and fibroblast responses are blunted in mice lacking gelsolin. Expression of nascent polypeptide-associated complex regulates formation of Fas-associated death domain (FADD) protein oligomers and modulates FADD-mediated signaling; FADD protein is a critical mediator of signal transduction pathways activated by several members of the tumor necrosis factor (TNF) receptor gene superfamily. Cathepsins are distinct intracellular acidic proteases that actively participate in the mechanism of antigen processing; conversely, the stefins are inhibitors of these cathepsins.

The immune response process is also statistically significantly induced in the lymphedema group versus controls. Proteins such as cytotoxic T lymphocyte-associated proteins are associated with activated T cell function and enhance TGF-β release by T cells [40]. Leukocyte (or lymphocyte) specific protein 1 (LSP1) is a multifunctional protein involved

Table 7. Functional Gene Expression Analysis in Experimental Lymphedema

Category	Upregulated	Fold Change	*q*-Value (%)	Downregulated	Fold Change	*q*-Value (%)
Acute inflammation	*calgranulin B*	22.5:1	2.729	*sphingosine kinase 1*	0.6:1	3.743
	S100 calcium binding protein A11	1.6:1	1.084	*gelsolin*	0.6:1	1.360
	tenascin C	7.8:1	0.913			
	lipocalin	6.1:1	0.913			
	stefin A3	4.3:1	0.913			
	proteoglycan, secretory granule	3.7:1	3.532			
	L-plastin 2	3.3:1	1.084			
	follistatin	3.2:1	1.084			
	procollagen type IV	3.0:1	2.729			
	arachidonate 5-lipoxygenase activating protein	2.9:1	1.587			
	stromal cell-derived factor 1	2.5:1	0.913			
	thymosin, beta 10	2.5:1	1.587			
	ferritin light chain 1	2.4:1	2.729			
	legumain	2.4:1	1.084			
	cathepsin C	2.3:1	1.587			
	cathepsin Z	2.2:1	1.084			
	cathepsin H	1.4:1	1.587			
	cathepsin L	1.5:1	4.279			
	glutathione peroxidase 1	1.9:1	1.084			
	platelet factor 4	1.9:1	1.084			
	lymphocyte specific 1	1.8:1	1.084			
	Basigin	1.7:1	4.029			
	thymosin, beta 4	1.7:1	3.238			
	CD63 antigen	1.5:1	3.730			
	nuclear factor of kappa light chain gene enhancer in B cells 1, p105	1.5:1	4.279			
	peptidylprolyl isomerase B	1.4:1	1.587			
	prosaposin	1.4:1	3.532			
	LPS-induced TNF-alpha factor	1.3:1	4.029			
	nascent polypeptide-associated complex alpha polypeptide	1.3:1	3.743			
Immune	*Lipocalin*	6.1:1	0.913	*oxysterol binding protein-like 1A*	0.6:1	4.029
	cytotoxic T lymphocyte-associated protein 2 alpha	4.5:1	0.913	*villin 2*	0.6:1	1.360
	Fc receptor, IgE, high affinity I, gamma polypeptide	4.2:1	0.913	*dual specificity phosphatase 14 (MAPK6)*	0.7:1	1.084
	beta-2 microglobulin	3.9:1	0.913	*nuclear factor 2*	0.7:1	3.730
	lectin, galactose binding, soluble 1	2.9:1	2.276	*CD2 antigen binding protein 2*	0.8:1	4.903
	legumain	2.4:1	1.084	*interferon regulatory factor 3*	0.8:1	4.029
	cathepsin C	2.3:1	1.587			
	cathepsin Z	2.2:1	1.084			
	cathepsin H	1.4:1	1.587			
	cathepsin L	1.5:1	4.279			
	interferon gamma receptor	2.0:1	0.913			
	lymphocyte specific 1	1.8:1	1.084			
	Granulin	1.7:1	1.084			
	interferon induced transmembrane protein 3-like	1.7:1	1.961			
	zinc finger protein 100	1.6:1	2.276			
	lymphocyte antigen 6 complex, locus E	1.6:1	2.729			
	interferon (alpha and beta) receptor 2	1.5:1	4.279			
Complement cascade	*histocompatibility 2, complement component factor B*	3.1:1	3.238			
	complement component 1, q subcomponent, c polypeptide	2.6:1	0.913			
	calreticulin	2.0:1	1.727			
	serine (or cysteine) proteinase inhibitor, clade I (neuroserpin), member 1	2.0:1	3.165			
Wound healing and fibrosis	*Tenascin C*	7.8:1	0.913	*gelsolin*	0.6:1	1.360
	Lipocalin	6.1:1	0.913			
	lysyl oxidase	2.7:1	1.727			
	Biglycan	2.6:1	3.165			
	thymosin, beta 10	2.5:1	1.587			
	procollagen, type V, alpha 2	2.4:1	3.730			
	fibulin 2	2.0:1	1.084			
	sorting nexin 5	2.0:1	1.084			
	platelet factor 4	1.9:1	1.084			
	actin, alpha 2, smooth muscle, aorta	1.7:1	4.279			

Table 7. Continued

Category	Upregulated	Fold Change	*q*-Value (%)	Downregulated	Fold Change	*q*-Value (%)
	Granulin	1.7:1	1.084			
	S100 calcium binding protein A11	1.6:1	1.084			
Stress response	*selenoprotein P*	2.8:1	2.276	*sterol regulatory element binding factor 1*	0.5:1	1.727
	selenoprotein K	1.3:1	3.743	*7-dehydrocholesterol reductase*	0.6:1	4.029
	selenoprotein W, muscle 1	2.2:1	4.903	*DnaJ (Hsp40) homolog, subfamily B, member 1*	0.6:1	3.238
	DnaJ (Hsp40) homolog, subfamily B, member 5	2.7:1	3.532	*malic enzyme, supernatant*	0.6:1	3.238
	ferritin light chain 1	2.4:1	2.729	*methylenetetrahydrofolate dehydrogenase (NAD^+ dependent), methenyltetrahydrofolate cyclohydrolase*	0.6:1	2.729
	fibulin 2	2.0:1	1.084	*glutathione S-transferase, alpha 4*	0.6:1	0.913
	glutathione peroxidase 1	1.9:1	1.084	*hydroxysteroid (17-beta) dehydrogenase 12*	0.7:1	1.360
	platelet factor 4	1.9:1	1.084			
	Carbonyl reductase 2	1.8:1	1.084			
	glyceraldehyde 3-phosphate dehydrogenase	1:6:1	3.730			
	heme oxygenase (decycling) 1	1.6:1	0.913			
	thioredoxin 1	1.6:1	3.730			
	chaperonin 10 (heat shock protein 1)	1.5:1	3.730			
	heat shock 70-kDa protein 8	1.5:1	4.029			
	superoxide dismutase 2	1:5:1	3.165			
	heat shock 70-kDa protein 2	1.4:1	4.279			
	heat shock 30-kDa protein	1.3:1	3.743			
	transaldolase 1	1.3:1	4.279			
Angiogenesis	*thymosin, beta 10*	2.5:1	1.587			
	hypoxia inducible factor 1, alpha subunit	1.9:1	1.961			
	triosephosphate isomerase	1.9:1	1.727			
	SRY-box containing gene 18 (SOX18)	1.8:1	4.029			
	endomucin	1.7:1	1.084			
	fibroblast growth factor binding protein	1.5:1	2.276			
Cytoskeletal	*caldesmon 1*	3.1:1	3.743	*gelsolin*	0.6:1	1.360
	thymosin, beta 10	2.5:1	1.587			
	actinin, alpha 1	1.8:1	2.729			
	calcium regulated heat stable protein 1	1.8:1	1.961			
	t-complex testis expressed 1	1.8:1	3.165			
	actin, alpha 2, smooth muscle, aorta	1.7:1	4.279			
	actin, beta, cytoplasmic	1.4:1	3.532			
	Basigin	1.7:1	4.029			
	capping protein beta 1	1.7:1	1.961			
	cofilin 1	1.7:1	4.029			
	Zyxin	1.6:1	3.743			
	actin related protein 2/3 complex, subunit 4	1.5:1	1.727			
	filamin-like	1.5:1	4.903			
	profilin 1	1.5:1	4.903			
	transgelin	1.5:1	2.729			
	ribosomal protein S18	1.2:1	1.961			
Wnt pathway	*Tenascin C*	7.8:1	0.913	*cadherin 1*	0.4:1	0.913
	receptor tyrosine kinase-like orphan receptor 2	1.7:1	1.587	*Notch gene homolog 1 (Drosophila)*	0.5:1	4.029
Adipogenesis	*fatty acid binding protein 5, epidermal*	2.2:1	2.729	*diacylglycerol O-acyltransferase 2*	0.5.1	1.084
	sorting nexin 5	2.0:1	1.084	*7-dehydrocholesterol reductase*	0.6:1	4.029
	esterase 10	1.9:1	1.084	*fatty acid synthase*	0.6:1	3.238
	SRY-box containing gene 18 (SOX18)	1.8:1	4.029	*3-hydroxy-3-methylglutaryl-coenzyme A reductase*	0.7:1	3.730
	coactosin	1.3:1	1.587			

DOI: 10.1371/journal.pmed.0030254.t007

in the regulation of neutrophil motility, chemotaxis, adhesion, and B lymphocyte apoptosis mediated by membrane immunoglobulin M (mIgM) [41]. Beta-2 microglobulin is a major histocompatibility complex protein that presents peptide antigens on cell surfaces for recognition by T cell receptors. Lipocalin has recently been shown to participate in the response to bacterial growth [42]. Galactose binding lectin is a participant in the acute phase response [43]. Granulin is a high-molecular-weight secreted mitogen that is abundantly expressed in rapidly cycling epithelial cells and in the immune system [44]. High affinity Fc receptor for IgE is a key molecule in triggering the allergic reaction; it might be considered to be a mast-cell-specific protein. Interferon gamma has an important role in activating macrophages in host defenses.

One of the most interesting findings of our study is that lymphedema mirrors many of the mechanisms of the inflammatory state, in the absence of a potent inflammatory stimulus. One would not necessarily hypothesize, a priori, that this would be the case, since the only difference between lymphedematous animals and the controls (both normals and surgical shams) was the presence of acute, acquired lymphatic

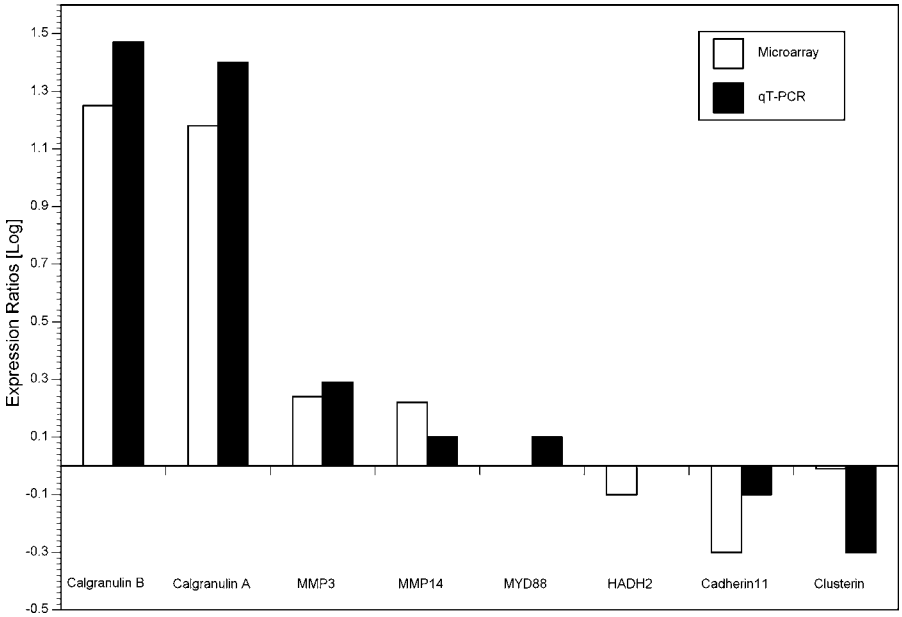

Figure 6. qRT-PCR Confirmation of the Results of Microarray Hybridization

The graph represents fold-changes of expression in lymphedema, relative to normal controls, for each of eight representative genes, by microarray hybridization and qRT-PCR. For *MYD88* by microarray and *HADH2* by qRT-PCR, the log (gene expression) equaled zero. *HADH2, hydroxysteroid (17-beta) dehydrogenase; 2MMP, matrix metalloproteinase; MYD88, myeloid differentiation primary response gene 88.*

DOI: 10.1371/journal.pmed.0030254.g006

stasis, with no additional inflammatory stimulus; thus, lymphatic stasis induces many of the same mechanisms as inflammatory stimuli. This important observation is novel and has led us to pursue follow-up investigation intended to determine the efficacy of inhibitors of the inflammatory pathways in reversing the pathologic responses of the tissues that are seen in lymphedema.

The apparent absence of lymphatic markers in this transcriptional profile suggests that, in principle, the findings might not be specific for lymphedema. However, in parallel work performed in the same animal model, we have identified several lymphatic markers including, most importantly, upregulation of VEGF-C (but not VEGF-A) and VEGFR-3. Therapeutic induction of a lymphangiogenic response through administration of exogenous, recombinant human VEGF-C produces both an amelioration of edema and a downregulation of both of these markers of the lymphatic vascular response to acquired vascular insufficiency (unpublished data). Finally, as seen in Figure 3, LYVE-1 staining demonstrates specific lymphatic vascular changes in this model, including an increase in lymphatic microvascular size and density, in response to induced lymphatic vascular disruption. None of the morphological, histochemical, or gene expression changes referred to here are observed in animals that are subjected to surgery in the absence of induction of specific lymphatic injury (surgical controls), as described in this paper. Thus, it reasonable to state that the histological and molecular responses reflect lymph stagnation and not the more nonspecific responses of wound healing after surgical injury.

The cellular response to stress is another process that undergoes statistically significant induction during lymph stagnation. Among the stresses that can trigger this response are the elaboration of pathophysiological signals such as cytokines and eicosanoids [45]. The expression of a variety of heat shock proteins is upregulated in our model [45]. Additional evidence for the oxidative stress in lymphatic dysfunction is provided by the upregulation of heme oxygenase 1 (HO-1) [46]; it is a downstream effector of the potent anti-inflammatory interleukin IL-10 [47].

Upregulation of gene expression related to wound repair, and importantly, to fibrosis is also prominently seen. During wound repair granulin promotes granulation and neovascularization, and regulates inflammation [48]. The expression of fibulins is induced in the setting of injury, in response to various stimuli [49]. Biglycan (BGN) has been implicated in the regulation of matrix assembly, cellular adhesion, migration, and TGF-β activity [50]. Endoglin (CD 105) is a type III TGF-β1 receptor. It modulates the function of TGF-β1 by binding to and modulating signal transduction by the major type I and II TGF-β1 receptors. Lysyl oxidase plays a critical role in the biogenesis of connective tissue matrices. Alpha 2 actin has been identified as a marker of myofibroblast differentiation; all fibrocontractive diseases characterized by fibrosis entail the presence of myofibroblasts [51].

In addition to inflammatory/immune and stress responses, we have observed a gene expression profile that reflects alterations in the angiogenic response**.** Specifically, hypoxia inducible factor 1α has a key role in the cellular response to hypoxia, including the regulation of genes involved in energy metabolism, angiogenesis, and apoptosis. Alterations in the complement and *Wnt* pathways may also contribute significantly to the pathogenesis of the skin response to lymph stasis.

The observed differences between the lymphedematous animals and the surgical controls are noteworthy. In the absence of any observed delay in wound healing, overt infection, or inflammation, the gene expression profile in

lymphedema, but not in surgical controls, is characterized by a remarkable induction of whole biological processes via coordinate upregulation of their component genes. These observations underscore the interpretation that lymphedema is a pathological process that is much more complex than a simple disorder of fluid homeostasis. Indeed, these gene expression profiles superficially resemble those of other recently elucidated inflammatory conditions, such as multiple sclerosis [31], psoriasis [52], and even atherosclerosis [53,54].

The differentially expressed genes in our study likely arise from a number of different cell types, including not only the cellular components of the inflammatory response, but also other involved cell types such as keratinocytes, vascular endothelial and smooth muscle cells, and fibroblasts. We feel that it is important to study the gene expression of cells within the complex cellular milieu of the damaged end organ in lymphedema, because precisely the genes we are interested in are those whose transcription results from cell–cell or cell–interstitial fluid interactions. When one removes cells from the milieu, there are immediate changes in transcription that are not reflective of the disease state. We are, of course, interested in defining the cellular compartments that are expressing specific genes, and this topic is the focus of ongoing research in our laboratory that will be published in the future.

In summary, we have used an animal model of lymphedema that shares many clinical and histopathological features with human lymphedema to identify the biological processes and genes that underlie these features. The fact that inflammatory and immune processes are significantly induced suggests that these observations will provide a useful avenue for the investigation of novel pharmacologic strategies for lymphatic dysfunction [2]. This approach is particularly attractive in light of the observed parallels with other systemic inflammatory disease states for which effective therapies already exist. Ultimately, such therapies must successfully diminish the impact of the soft tissue fibrosis and adipose deposition that characterize the late disease [2]; in this regard, it is interesting to contemplate that expression of several such genes is detectably altered in this model, long before architectural evidence of the tissue abnormality is present. This identification of such genes provides an avenue for future investigation and, specifically, provides early insights into the elaboration of molecular therapeutics for this disease. Our purpose here has been to establish an animal model that can be used in two ways: first, to generate new hypotheses about unsuspected genes and pathways that are involved in lymphedema and, second, to eventually test potential pharmacologic and therapeutic interventions for their efficacy in vivo. We recognize that not all interventions that show promise in animal models translate effectively into treatments for human disease, but such in vivo testing is an essential prerequisite to human application and testing, and the establishment of a good, relatively inexpensive animal model is a very important step in allowing more high-throughput analysis of putative therapeutic interventions. These studies contribute to our understanding of the pathogenesis of lymphedema. Further characterization of the genes and molecular pathways identified through this effort will likely provide insights into potential novel strategies for molecular therapies.

Supporting Information

Table S1. Annotated List of the cDNAs Included on the Mouse Transcriptome Microarray Utilized in These Investigations

Found at DOI: 10.1371/journal.pmed.0030254.st001 (75.6 MB HTM).

Accession Numbers

The microarray data from these investigations have been deposited as dataset GSE4333 in the Gene Expression Omnibus database (http://www.ncbi.nlm.nih.gov/geo). Accession numbers for the genes and proteins referenced in tables refer to the LocusLink database (http://www.ncbi.nlm.nih.gov/projects/LocusLink).

Acknowledgments

The authors gratefully acknowledge grant support from the Susan G. Komen Breast Cancer Foundation and the Western States Affiliate of the American Heart Association.

Author contributions. RT, AB, and SGR participated in study design. RT, JS, NR, and RW participated in microarray execution and analysis. AA and NR participated in the execution of RT-PCR. LC and SSD participated in histological preparation and analysis. JH, AB, and SJ participated in imaging execution and data analysis. JH participated in microsphere techniques. JH participated in immunohistochemistry. SSD participated in LYVE-1 immunohistochemistry. RT, LC, AB, AD, SJ, and SGR participated in data analysis. RT, LC, and SGR participated in manuscript preparation.

References

1. Szuba A, Rockson S (1997) Lymphedema: Anatomy, physiology and pathogenesis. Vasc Med 2: 321–326.
2. Rockson SG (2001) Lymphedema. Am J Med 110: 288–295.
3. Piller NB (1990) Macrophage and tissue changes in the developmental phases of secondary lymphoedema and during conservative therapy with benzopyrone. Arch Histol Cytol 53: 209–218.
4. Olszewski WL, Engeset A, Romaniuk A, Grzelak I, Ziolkowska A (1990) Immune cells in peripheral lymph and skin of patients with obstructive lymphedema. Lymphology 23: 23–33.
5. Beilhack A, Rockson SG (2003) Immune traffic: A functional overview. Lymphat Res Biol 1: 219–234.
6. Podgrabinska S, Braun P, Velasco P, Kloos B, Pepper M, et al. (2002) Molecular characterization of lymphatic endothelial cells. Proc Natl Acad Sci U S A 99: 16069–16074.
7. Hirakawa S, Hong YK, Harvey N, Schacht V, Matsuda K, et al. (2003) Identification of vascular lineage-specific genes by transcriptional profiling of isolated blood vascular and lymphatic endothelial cells. Am J Pathol 162: 575–586.
8. Shin WS, Szuba A, Rockson SG (2003) Animal models for the study of lymphatic insufficiency. Lymphat Res Biol 1: 159–169.
9. Tabibiazar R, Quertermous T (2003) Use of high throughput genomic tools for the study of endothelial cell biology. Lymphat Res Biol 1: 133–145.
10. Sitzia J (1995) Volume measurement in lymphoedema treatment: Examination of formulae. Eur J Cancer Care (Engl) 4: 11–16.
11. Cao YA, Wagers AJ, Beilhack A, Dusich J, Bachmann MH, et al. (2004) Shifting foci of hematopoiesis during reconstitution from single stem cells. Proc Natl Acad Sci U S A 101: 221–226.
12. Beilhack A, Schulz S, Baker J, Beilhack GF, Wieland CB, et al. (2005) In vivo analyses of early events in acute graft-versus-host disease reveal sequential infiltration of T-cell subsets. Blood 106: 1113–1122.
13. Reinhardt CP, Dalhberg S, Tries MA, Marcel R, Leppo JA (2001) Stable labeled microspheres to measure perfusion: Validation of a neutron activation assay technique. Am J Physiol Heart Circ Physiol 280: H108–H116.
14. Tabibiazar R, Wagner RA, Liao A, Quertermous T (2003) Transcriptional profiling of the heart reveals chamber-specific gene expression patterns. Circ Res 93: 1193–1201.
15. Wagner Laboratory (2006) MouseDevelopment.org [database]. Stanford (California): Stanford University School of Medicine Division of Cardiovascular Medicine. Available: http://mousedevelopment.org. Accessed 24 May 2006.
16. Stanford Functional Genomics Facility (2006) Stanford Functional Genomics Facility [database]. Available: http://microarray.org. Accessed 5 June 2006.
17. Stanford Microarray Database (2006) Stanford Microarray Database [database]. Available: http://smd.stanford.edu. Accessed 24 May 2006.
18. Troyanskaya O, Cantor M, Sherlock G, Brown P, Hastie T, et al. (2001) Missing value estimation methods for DNA microarrays. Bioinformatics 17: 520–525.
19. Tusher VG, Tibshirani R, Chu G (2001) Significance analysis of microarrays

applied to the ionizing radiation response. Proc Natl Acad Sci U S A 98: 5116–5121.
20. Stanford University Department of Statistics (2006) SAM: Significance Analysis of Microarrays [computer program]. Standford (California): Stanford University Department of Statistics. Available: http://www-stat.stanford.edu/~tibs/SAM. Accessed 5 June 2006.
21. Quertermous Laboratory (2006) HeatMap Builder [computer program]. Stanford (California): Stanford University School of Medicine Division of Cardiovascular Medicine. Available: http://mozart.stanford.edu/heatmap.htm. Accessed 24 May 2006.
22. Chen MM, Ashley EA, Deng DX, Tsalenko A, Deng A, et al. (2003) Novel role for the potent endogenous inotrope apelin in human cardiac dysfunction. Circulation 108: 1432–1439.
23. Hosack DA, Dennis G Jr, Sherman BT, Lane HC, Lempicki RA (2003) Identifying biological themes within lists of genes with EASE. Genome Biol 4: R70.
24. Banerji S, Ni J, Wang SX, Clasper S, Su J, et al. (1999) LYVE-1, a new homologue of the CD44 glycoprotein, is a lymph-specific receptor for hyaluronan. J Cell Biol 144: 789–801.
25. Jackson DG (2004) Biology of the lymphatic marker LYVE-1 and applications in research into lymphatic trafficking and lymphangiogenesis. APMIS 112: 526–538.
26. Wilson SF (2004) Histopathologic improvement with lymphedema management, Leogane, Haiti. Emerg Infect Dis 10: 1938–1946.
27. Ristimaki A, Narko K, Enholm B, Joukov V, Alitalo K (1998) Proinflammatory cytokines regulate expression of the lymphatic endothelial mitogen vascular endothelial growth factor-C. J Biol Chem 273: 8413–8418.
28. Mouta C, Heroult M (2003) Inflammatory triggers of lymphangiogenesis. Lymphat Res Biol 1: 201–218.
29. Chi JT, Chang HY, Haraldsen G, Jahnsen FL, Troyanskaya OG, et al. (2003) Endothelial cell diversity revealed by global expression profiling. Proc Natl Acad Sci U S A 100: 10623–10628.
30. Kunz M, Ibrahim SM, Koczan D, Scheid S, Thiesen HJ, et al. (2004) DNA microarray technology and its applications in dermatology. Exp Dermatol 13: 593–606.
31. Lock C, Hermans G, Pedotti R, Brendolan A, Schadt E, et al. (2002) Gene-microarray analysis of multiple sclerosis lesions yields new targets validated in autoimmune encephalomyelitis. Nat Med 8: 500–508.
32. Ashburner M, Ball CA, Blake JA, Botstein D, Butler H, et al. (2000) Gene ontology: Tool for the unification of biology. The Gene Ontology Consortium. Nat Genet 25: 25–29.
33. Ryckman C, Vandal K, Rouleau P, Talbot M, Tessier PA (2003) Proinflammatory activities of S100: Proteins S100A8, S100A9, and S100A8/A9 induce neutrophil chemotaxis and adhesion. J Immunol 170: 3233–3242.
34. Eckert RL, Broome AM, Ruse M, Robinson N, Ryan D, et al. (2004) S100 proteins in the epidermis. J Invest Dermatol 123: 23–33.
35. Chiquet-Ehrismann R, Chiquet M (2003) Tenascins: Regulation and putative functions during pathological stress. J Pathol 200: 488–499.
36. Bukrinsky MI (2002) Cyclophilins: Unexpected messengers in intercellular communications. Trends Immunol 23: 323–325.
37. Bleul CC, Fuhlbrigge RC, Casasnovas JM, Aiuti A, Springer TA (1996) A highly efficacious lymphocyte chemoattractant, stromal cell-derived factor 1 (SDF-1). J Exp Med 184: 1101–1109.
38. Barreda DR, Hanington PC, Walsh CK, Wong P, Belosevic M (2004) Differentially expressed genes that encode potential markers of goldfish macrophage development in vitro. Dev Comp Immunol 28: 727–746.
39. Jones KL, de Kretser DM, Patella S, Phillips DJ (2004) Activin A and follistatin in systemic inflammation. Mol Cell Endocrinol 225: 119–125.
40. Chen W, Wahl SM (2003) TGF-beta: The missing link in CD4+CD25+ regulatory T cell-mediated immunosuppression. Cytokine Growth Factor Rev 14: 85–89.
41. Wong MJ, Malapitan IA, Sikorski BA, Jongstra J (2003) A cell-free binding assay maps the LSP1 cytoskeletal binding site to the COOH-terminal 30 amino acids. Biochim Biophys Acta 1642: 17–24.
42. Flo TH, Smith KD, Sato S, Rodriguez DJ, Holmes MA, et al. (2004) Lipocalin 2 mediates an innate immune response to bacterial infection by sequestrating iron. Nature 432: 917–921.
43. Peng X, Wu Y, Chen J, Wang S (2004) Proteomic approach to identify acute phase response-related proteins with low molecular weight in loach skin following injury. Proteomics 4: 3989–3997.
44. Ong CH, Bateman A (2003) Progranulin (granulin-epithelin precursor, PC-cell derived growth factor, acrogranin) in proliferation and tumorigenesis. Histol Histopathol 18: 1275–1288.
45. Lin KM, Hollander JM, Kao VY, Lin B, Macpherson L, et al. (2004) Myocyte protection by 10 kD heat shock protein (Hsp10) involves the mobile loop and attenuation of the Ras GTP-ase pathway. FASEB J 18: 1004–1006.
46. Takahashi T, Morita K, Akagi R, Sassa S (2004) Heme oxygenase-1: A novel therapeutic target in oxidative tissue injuries. Curr Med Chem 11: 1545–1561.
47. Lee TS, Chau LY (2002) Heme oxygenase-1 mediates the anti-inflammatory effect of interleukin-10 in mice. Nat Med 8: 240–246.
48. He Z, Bateman A (2003) Progranulin (granulin-epithelin precursor, PC-cell-derived growth factor, acrogranin) mediates tissue repair and tumorigenesis. J Mol Med 81: 600–612.
49. Argraves WS, Greene LM, Cooley MA, Gallagher WM (2003) Fibulins: Physiological and disease perspectives. EMBO Rep 4: 1127–1131.
50. Ungefroren H, Lenschow W, Chen WB, Faendrich F, Kalthoff H (2003) Regulation of biglycan gene expression by transforming growth factor-beta requires MKK6-p38 mitogen-activated protein kinase signaling downstream of Smad signaling. J Biol Chem 278: 11041–11049.
51. Chaponnier C, Gabbiani G (2004) Pathological situations characterized by altered actin isoform expression. J Pathol 204: 386–395.
52. Terui T (2000) Inflammatory and immune reactions associated with stratum corneum and neutrophils in sterile pustular dermatoses. Tohoku J Exp Med 190: 239–248.
53. Tabibiazar R, Wagner RA, Ashley EA, King JY, Ferrara R, et al. (2005) Signature patterns of gene expression in mouse atherosclerosis and their correlation to human coronary disease. Physiol Genomics 22: 213–226.
54. Tabibiazar R, Wagner RA, Spin JM, Ashley EA, Narasimhan B, et al. (2005) Mouse strain-specific differences in vascular wall gene expression and their relationship to vascular disease. Arterioscler Thromb Vasc Biol 25: 302–308.

Editors' Summary

Background. Lymphedema is the term used to describe the swelling that can occur after surgery, especially after axillary lymph node dissection for breast cancer, when the lymph vessels that carry protein-rich interstitial fluid from the tissues to the heart are damaged. Lymphedema can be extremely unpleasant and is very hard to treat; treatments that are currently used include those aimed to help massage the flow of lymph back to the chest. Lymphedema seems to be more than just accumulation of lymph, however, as changes also occur in the tissue surrounding the damaged lymph vessels. Currently, very little is known at the most basic level about what exactly these changes are, although they appear to be similar to an inflammatory process. One way of studying such a disease process in humans is to make an animal model that mimics the human condition and study the changes that occur there. For lymphedema, such a model can be made in the mouse tail by cutting lymph vessels there.

Why Was This Study Done? The authors wanted to look closely at what happens in the tissues surrounding damaged lymph vessels to try to understand better what these changes are. They also wanted to study the movement of the cells that are normally carried in the lymph.

What Did the Researchers Do and Find? The mouse model that the authors developed closely simulates the characteristics of human acquired lymphedema. In the mouse tails that had had their lymph vessels damaged, the authors were able to show that the tails were swollen compared with those of normal animals and of animals that hadhad sham (pretend) surgery. In the animals with lymphedema, many small lymph vessels were seen, as the lymph was unable to flow away normally. The area affected by the lymphedema had the appearance often seen in inflamed tissue, and analysis of genes from the same area to see how active, or "expressed," they were showed changes that are often seen in, for example, acute inflammation and wound healing. The authors also showed that when these animals were injected with immune cells marked with a light marker, they were less able to remove the cells from the circulation.

What Do These Findings Mean? These results show that the response to lymph stagnation is complex, but looks similar to that seen in acute inflammation. These results and this model may be useful in suggesting, and at a later date perhaps testing, treatments for lymphedema. One difference, however, between this mouse model and the condition in humans is that whereas lymphedema in humans is a rather chronic condition, here the researchers were only able to look at the changes over a short period of time. In a related Perspective article, Peter Carmeliet and colleagues further discuss the clinical relevance of these findings (http://dx.doi.org/10.1371/journal.pmed.0030264).

Additional Information. Please access these Web sites via the online version of this summary at http://dx.doi.org/10.1371/journal.pmed.0030254.

- The National Cancer Institute has information for patients and health professionals on lymphedema
- Cancerbackup is a United Kingdom cancer information service with information on many aspects of cancer, including lymphedema
- The Lymphatic Research Foundation Description has information on lymphatic system research